International Journal of Analysis and Applications

Applying Quadri-Partition Neutrosophic Soft Locally Compact Spaces to Enhance Machine Learning and Uncertainty Management

Haitham Qawaqneh[1], Dragan Pamucer[2,*], Raed Hatamleh[3], Mohamed Said Mohamed[4,5], Hamza Ali Abujabal[6], Arif Mehmood[7], Rabia Andleeb[7], Jamil J. Hamja[8], Cris L. Armada[9,10]

[1]*Al-Zaytoonah University of Jordan, Amman 11733, Jordan*

[2*]*Széchenyi István University, Győr, Hungary*

[3]*Department of Mathematics, Faculty of Science, Jadara University, P.O. Box 733, Irbid 21110, Jordan*

[4]*Department of Mathematics, College of Science and Humanities, Prince Sattam bin Abdulaziz University, Hawtat Bani Tamim 16511, Saudi Arabia*

[5]*Mathematics Department, Faculty of Education, Ain Shams University, Cairo 11341, Egypt*

[6]*Department of mathematics, King Abdulaziz University, P.O. Box 80003, Jeddah 21580, Saudi Arabia*

[7]*Department of Mathematics, Institute of Numerical Sciences, Gomal University, Dera Ismail Khan 29050, KPK, Pakistan*

[8]*Mathematics and Sciences Department, College of Arts and Sciences, MSU - Tawi-Tawi College of Technology and Oceanography, 7500 Philippines*

[9]*National University Ho Chi Minh City, Linh Trung Ward, Thu Duc City, Ho Chi Minh City, Vietnam*

[10]*Department of Applied Mathematics, Faculty of Applied Science, Ho Chi Minh City University of Technology (HCMUT), 268 Ly Thuong Kiet, Ward 14, District 10, Ho Chi Minh City, Vietnam*

**Corresponding author: pamucar.dragan@sze.hu*

Abstract. Within the broader framework of quadri-partition neutrosophic soft bi-topological spaces (QPNSBTS), the concept of quadri-partition neutrosophic soft locally compact space (QPNSLCS) is introduced in this research. It strengthens the theoretical foundation for handling uncertainty in complex topological structures by demonstrating that local compactness, particularly when combined with the Hausdorff requirement, entails the existence of compact neighbors and compactness in subspaces. The key concepts and theorems illustrate how compactness can be

Received Sep. 16, 2025

2020 Mathematics Subject Classification. 03E72.

Key words and phrases. neutrosophic soft sets; QPNSLCS; QPNSTS; tangent similarity; machine learning techniques.

https://doi.org/10.28924/2291-8639-24-2026-38

ISSN: 2291-8639

effectively used in the context of neutrosophic soft sets, which are a more powerful way to handle unclear and ambiguous data in advanced mathematical and practical applications. Furthermore, a number of machine learning algorithms are used to explore the concept of a tangent similarity between two quadri-partition neutrosophic soft sets. Additionally, the current study includes a number of studies and visualizations to evaluate the effectiveness of different clustering algorithms and dimensionality reduction techniques. Each of the graphics in the findings illustrates a distinct method for viewing and comprehending complex data. The K-means++ initialization (Fig. 6.1) serves as an illustration of how the algorithm's initialization step improves clustering accuracy by choosing centroid (data points) that are widely distributed, reducing the likelihood of subpar clustering performance. More training is required since hidden units are only activated with low activations, according to restricted Boltzmann Machine (RBM) activation patterns (Fig. 6.2). Additionally, the Linear Discriminant Analysis (LDA) plots (Fig. 6.4) and Heatmaps (Fig. 6.3) might provide helpful details regarding the organization and segregation of the datasets. The discussion of the results, which can be devoted to their applicability in terms of clustering, dimensionality reduction, and feature learning, is based on these methods and the associated visual models.

1. Introduction

A primary focus of computational intelligence has been the search for reliable mathematical models to describe the prevalent uncertainty and indeterminacy of real-world decision-making situations. This journey began with Zadeh's groundbreaking work on fuzzy set theory [1], which elegantly expanded on classical set theory by introducing the concept of membership grades, allowing for the representation of imprecise data. The generalization of this word into intuitionistic fuzzy sets (IFS), where each element is specified in terms of a membership level (μ) and non-membership level (ν), was another way to extend the human tendency toward hesitation. A similar pattern emerged concurrently with Molodtsov's novel theory of soft sets [3], which addressed parametric uncertainties by mapping a collection of parameters to subsets of a universal set. When Maji, Biswas, and Roy [4] presented the idea of fuzzy soft sets, creating a versatile hybrid model in the treatment of imprecision as well as parameterization, the fusion of the two significant paradigms became a reality. A plethora of hybrid models, including interval-valued vague soft sets [6], vague soft sets [5], and soft expert sets [7], were developed as a result of this combination, each of which added expressiveness to certain application domains. Smarandache created the broad generalization of neutrosophy [8] and the associated idea of the neutrosophic set [9]. This paradigm offers a unique ability to deal with contradictory, indeterminate, and incomplete information since it explicitly treats the degree of truth-membership (T), indeterminacy-membership (I), and falsity-membership (F) separately, going beyond previous models.

Maji's groundbreaking concept of the neutrosophic soft set (NSS) [10] was the next step in fusing neutrosophy and soft set theory. This excellent structure makes advantage of the representational power of neutrosophy and the parametric flexibility of soft sets to provide a comprehensive model of uncertain data where the simultaneous judgment of parameters is truth, indeterminacy, and falsity. Numerous academics have expanded NSS's theoretical and

practical foundation. Deli and Broumi's [11] growth of the theory into neutrosophic soft matrices and a decision-making process, as well as Deli's [12] transition to the interval-valued space to express finer imprecision, serve as examples. Alkhazaleh [13] introduced time-neutrosophic soft sets to address the dynamic of real-world situations. The element of relations that form the basis of logical reasoning and multi-attributes decision-making (MADM) is at the heart of the application of these set theories. Relationship The fuzzy relation [14], intuitionistic fuzzy soft relation, neutrosophic soft relation, and single-valued neutrosophic relations [16,17] are the sets that the relation study has evolved alongside. These relational structures provide the tools required to specify functions and the structure of sophisticated algorithms. This study introduces a novel idea, the Complex Neutrosophic Soft Expert Relation, which is based on this outstanding background. This novel framework combines the two-dimensional geometry of complex numbers, the evaluative power of expert sets, the parametricity of soft sets, and the three-dimensional analysis of certainty of neutrosophic sets. By doing this, it provides a clear and efficient mathematical language to organize complex, time-sensitive, and expert decision-making problems under uncertainty, with the ultimate goal of enhancing the precision and reliability of outcomes in domains such as computer-aided reasoning, artificial intelligence, and information retrieval. Classical results have been extended to b-metric, fuzzy, and fractional metric spaces by more recent studies in fixed point theory [42,43,46]. Through the introduction of novel contractions and functions, this study provides the structures for proving the existence and uniqueness of the solutions [45]. This is directly used to nonlinear models and fractional various equations [41,44], which is beneficial both theoretically and practically. Modern problems necessitate sophisticated computational techniques. Modern problems necessitate sophisticated computational techniques. As Elbes et al. [47] have shown with reference to COVID-19 identification based on X-rays, deep learning can be utilized to perform strong diagnostics in healthcare. The ability of IoT technology to transform the educational environment was also demonstrated by Kanan et al. [48]. Using a fractional-order PID controller as the foundation for these applications, Batiha et al. [49] offered precise control of robotic systems.

Literature Review: Applications of neutrosophic sets

First put forth by Florentin Smarandache, the neutrosophic logic is a mathematical paradigm that has emerged as a ground-breaking technique for characterizing ambiguity, inconsistency, and uncertainty in a wide range of domains. Truth (T), indeterminacy (I), and falsity (F) are the three independent membership functions that describe information according to this theory. As a result, several generalizations have been developed and are increasingly being used in practical contexts. Relevance In the fields of medicine, engineering, the military, image processing, and computer science, standard neutrosophic sets and their generalizations—such

as neutrosophic soft sets, refined neutrosophic sets, and double-valued neutrosophic sets—have been applied to solve real-world issues that are marked by imprecision and incomplete information. In the medical field, neutrosophic sets and single-valued neutrosophic sets have been used to enhance the diagnostic procedure. These models allow symptoms to be represented in an ambiguous way, which allows similarity measures to be used to match patient data to known disease phenotypes. This allows doctors to handle incomplete or mismatched data [18].

When more than one expert and more than one parameter are taken into account, such as when selecting the best treatment alternatives by adding up the evaluations based on several parameters like cost, efficacy, and side effects, the neutrosophic soft set extension is very helpful [20]. Refined neutrosophic sets offer a finer granularity in increasingly complicated biological data and divide indeterminacy into sub-parts like uncertainty and contradiction. This is especially important in genomic studies, where the level of gene expression may be caused by noise or contradicting evidence [21].

Neutrosophic methods are also helpful in military and engineering settings. In engineering applications, the neutrosophic sets are utilized to record unknown failure reasons or supplier performance metrics, as well as to undertake reliability analysis and supply chain decisions [22]. The same ideas are used in military operations to evaluate the dangers and make judgments in the command situation by differentiating between information that has been confirmed to be accurate, information that has not been verified, and misinformation, which is a realistic representation of the fog of war [23]. Double-valued neutrosophic sets, which can introduce two perspectives, can also be used to expand these applications. For instance, in fault diagnosis, one value can be used to indicate the degree of confidence and another to indicate the severity of the problem, leading to more robust engineering systems [25]. Similar to this, military intelligence's dual-valued measurements enhance situational awareness by allowing the integration of information from many sources, including satellite photography and human agents [24]. Neutrosophic theory has important implications for signal and image processing. In this instance, advanced segmentation and denoising algorithms can be implemented using neutrosophic sets, where pixels are transformed into a space where indeterminacy is a clear indicator of noise and uncertainty. This approach has shown more effective than traditional fuzzy algorithms in processing medical imaging, such as CT and MRI scans, where noise poses a significant challenge to accurate diagnosis [26, 27]. These characteristics are further enhanced by refined neutrosophic sets, which enable more precise and practical picture augmentation algorithms and can discriminate between categories of indeterminacy, such as cloud cover and sensor noise in satellite imagery [21]. Science of computers Work on decision-making and computational intelligence uses neutrophilic systems. Neutrosophic soft sets serve as the

foundation for sophisticated multi-criteria decision-making models, which are employed in domains like human resource allocation, where subjective assessments vary, and recommender systems, where user preferences are not always predetermined [20, 28]. Apart from soft sets, standard neutrosophic sets are helpful in building robust machine learning. For example, AI systems that can reason with ambiguous data and neutrosophic clustering algorithms that use indeterminacy degrees to work with noisy data are examples of how machine learning can become more like human reasoning [29, 30].

Overall, the literature shows how neutrosophic sets and their generalizations can be used to solve challenging real-world issues in a variety of fields. These tools continue to support advancements in data science, healthcare, defense, and technology by providing a methodical yet flexible approach to modeling and handling uncertainties, confirming their growing importance in both theoretical and applied research. Recent advancements in multi-criteria decision-making (MCDM) have increasingly focused on enhanced uncertainty modeling and more flexible preference designs. Numerous cutting-edge methods, such as Hyper-fuzzy VIKOR and DEMATEL, have improved the analytical capabilities of traditional MCDM frameworks [34]. At the same time, interval-valued Fermatean neutrosophic super hyper structures have provided strong solutions to complex decision-making environments, particularly in healthcare [35]. Moreover, the ranking and assessment systems are still enhanced by bipolar fuzzy preference models using protracted VIKOR-based approaches [36]. At the same time, significant progress has been made in the analytical and numerical principles of neutrosophic and fuzzy systems. New numerical techniques have been employed to enhance the solvability of neutrosophic singular boundary value problems, including LPM-based polynomial methods [37]. Additionally, graph-theoretic methods have been applied to deepen the understanding of threshold conversion dynamics in neutrosophic structures [38].

Additional contributions include new trigonometric and weighted operator-based frameworks of (gamma, tau)-rung fuzzy sets [39], as well as new topological constructions derived from symbolic n-plithogenic intervals [40]. Alongside these developments, novice researchers in topological superconductors continue to demonstrate the applicability of sophisticated mathematical models in supporting cutting-edge physical applications [50].

Motivation for research

The literature does not presently contain any neutrosophic set applications that use the IRIS dataset and incorporate the following techniques:

1. Principal Component Analysis (PCA) of IRIS Data: PCA reduces the number of dimensions in a dataset by breaking down features into orthogonal components. Neutrosophic PCA can capture non-determinate correlations between the features or uncertainty in the contribution of variances.

2. t-SNE (t-Distributed Stochastic Neighbor Embedding) of IRIS Data: t-SNE shows high-dimensional data in 2D/3D. By permitting truth, indeterminacy, and falsity memberships in similarity calculations, a neutrosophic t-SNE could address cluster membership ambiguity.
3. Using K-Means++ to cluster IRIS data: K-Means++ improves on initial centroid selection. Cluster validity may be eliminated when neutrophilic K-Means++ divides the data points into groups with membership, indeterminacy, and non-membership degrees.
4. IRIS Data and the RBM (Restricted Boltzmann Machine) Hidden Layer: Generative neural networks, or RBMs, are used to learn features. Neutrosophic units, which are hidden units that explain unclear activations, can be modeled using a neutrosophic RBM.
5. Global Linear Optimization, or GLO IRIS Data: GLO is utilized globally to solve linear issues. It is possible to optimize under indeterminate parameters by using neutrosophic constraints.
6. IRIS Data with Latent Dirichlet Allocation (LDA): Although LDA is usually used in text, it may also be used to model features and space subjects. Neutrosophic LDA could be topic-modelling features whose topic assignments are non-determinate.
7. IRIS Data Independent Component Analysis (ICA): ICA is a technique for breaking down mixed signals into their component parts. The issue of component independence or indeterminacy in mixing matrices may be resolved via neutrophilic ICA.
8. IRIS Data (Normalized)- K-Means Clustering: Scales the features, however, neutrosophic K-Means can also deal with uncertainty in scaled values or cluster allocations..
9. Static visualizations of distributions are called bar graphs and 3D bar graph plots. The memberships of truth, indeterminacy, and falsehood in classes or features could be visualized via neutrophilic versions.
10. Parallel Coordinates in 3D t-SNE: Multivariate data is displayed using the parallel coordinates. Their cross-dimensional trajectories would be uncertain when using neutrosophic t-SNE.
11. Spline and Original Points Splines balance the patterns in data movement in a smooth function curve. Neutrosophic splines could be used to model curves with an unknown smoothing parameter or the undetermined fits.
10. IRIS Data FPCA: PCA is extended to functional data using FPCA. Neutrosophic FPCA can be used to determine the Eigen-functions of a given functional under unknown functional observations.

Novelty of research

Presenting Quadri-partition Neutrosophic Soft Locally Compact Spaces (QPNSLCS) inside the context of QPNSTS, a novel approach to the issue of uncertainty and indeterminacy in topological structures, is what makes this segment distinctive.

Local compactness with the Hausdorff condition, which ensures the preservation of the compact neighborhoods within the subspaces, and the variety of data visualization techniques, such as K-means++, RBM, Heatmaps, LDA, and ICA, are the results of the study. Data points and their categories are further understood through the use of color mappings and number tables in the study's clear and detailed visuals, which analyze linkages and patterns in complicated datasets. Combining these methods on a single research offers a comprehensive approach to feature analysis, clustering, and data representation that is uncommon in a single framework.

2. Preliminaries

This segment addresses the basic functions

To begin with, the idea of neutrosophic soft sets was first established by Maji [20]. Later, Deli and Bromi [16] refined and modified this concept, as detailed below:

Definition 2.1. É represents a collection of parameters, and Ũ denotes an initial universe set. $P(Ũ)$ denotes the set of all NSs for Ũ. A set defined by a set valued function $F̃$ that represents a mapping of the form $F̃ : É \to P\ (Ũ)$ is called NSS $(F̃, É)$ over Ũ, with $F̃$ being the approximate function of this NSS. In other terms, the NSS can be described as a set of ordered pairs, $(F̃, É) = \{(e, \langle x, T_{F̃(e)}(x), I_{F̃(e)}(x), F_{F̃(e)}(x)\rangle : x \in Ũ) : e \in É\}$.

$T_{F̃(e)}(x), I_{F̃(e)}(x), F_{F̃(e)}(x) \in [0,1]$ are the truth, indeterminacy, and falsity-membership functions of $F̃(e) \in [0,1]$.The inequality$0 \le T_{F̃(e)}(x) + I_{F̃(e)}(x) + F_{F̃(e)}(x) \le 3$ is clear since the supremum of each T, I, and F is 1.

Definition 2.2. [31] Let $(F̃, É)$ be NSS. $(F̃, É)^c$ *is complement* of $(F̃, É)$

$(F̃, É)^c = \{(e, \langle x, F_{F̃(e)}(x), 1 - I_{F̃(e)}(x), T_{F̃(e)}(x)\rangle : x \in Ũ) : e \in É\}$

Obvious that, $((F̃, É)^c)^c = (F̃, É)$.

Definition 2.3 [32] Let $(F̃, É)$ and $(G̃, É)$ be two NSSs. $(F̃, É) \tilde{\subseteq} (G̃, É)$ if $T_{F̃(e)}(x) \le T_{G̃(e)}(x), I_{F̃(e)}(x) \le I_{G̃(e)}(x), F_{F̃(e)}(x) \ge F_{G̃(e)}(x) \forall e \in É, \forall x$.

Definition 2.4 [32] Let $(\widetilde{F_1}, É)$ and $(\widetilde{F_2}, É)$ be two NSSs. Then union of these sets is denoted by $(\widetilde{F_1}, É) \cup (\widetilde{F_2}, É) = (\widetilde{F_3}, É)$ with

$$(\widetilde{F_3}, É) = \{(e, \langle x, T_{F̃_3(e)}(x), I_{F̃_3(e)}(x), F_{F̃_3(e)}(x)\rangle : x \in Ũ) : e \in É\}$$

Where

$$\begin{cases} T_{F̃3(e)}(x) &= max\{T_{F̃_1(e)}(x), T_{F̃_2(e)}(x)\}, \\ I_{F̃3(e)}(x) &= max\{I_{F̃_1(e)}(x), I_{F̃_2(e)}(x)\}, \\ F_{F̃3(e)}(x) &= min\{F_{F̃_1(e)}(x), F_{F̃_2(e)}(x)\}. \end{cases}$$

Definition 2.5 [32] Let $(\widetilde{F_1}, É)$ and $(\widetilde{F_2}, É)$ be two NSSs. Then intersection of these sets is symbolized by $(\widetilde{F_1}, É) \cap (\widetilde{F_2}, É) = (\widetilde{F_3}, É)$ with

$$(\widetilde{F_3}, É) = \{(ę, \langle x̧, T_{\tilde{F}_3(ę)}(x̧), I_{\tilde{F}_3(ę)}(x̧), F_{\tilde{F}_3(ę)}(x̧)\rangle : x̧ \in Ũ) : ę \in É\}$$

Where

$$\begin{cases} T_{\tilde{F}3(e)}(x̧) = min\{T_{\tilde{F}_1(ę)}(x̧), T_{\tilde{F}_2(ę)}(x̧)\}, \\ I_{\tilde{F}3(e)}(x̧) = min\{I_{\tilde{F}_1(ę)}(x̧), I_{\tilde{F}_2(ę)}(x̧)\}, \\ F_{\tilde{F}3(e)}(x̧) = max\{F_{\tilde{F}_1(ę)}(x̧), F_{\tilde{F}_2(ę)}(x̧)\}. \end{cases}$$

Definition 2.6 [32] Let $(\widetilde{F_1}, É)$ and $(\widetilde{F_1}, É)$ are NSSs. Then $(\widetilde{F_1}, É)\backslash(\widetilde{F_2}, É)$ is denoted by $(\widetilde{F_1}, É)\backslash (\widetilde{F_2}, É) = (\widetilde{F_3}, É)$ with

$$(\widetilde{F_3}, É) = \{(ę, \langle x̧, F_{\tilde{F}_3(ę)}(x̧), I_{\tilde{F}_3(ę)}(x̧), F_{\tilde{F}_3(ę)}(x̧)\rangle : x̧ \in Ũ) : ę \in É\}$$

Where

$$\begin{cases} T_{\tilde{F}3(e)}(x̧) = min\{T_{\tilde{F}_1(ę)}(x̧), F_{\tilde{F}_2(ę)}(x̧)\}, \\ I_{\tilde{F}3(e)}(x̧) = min\{I_{\tilde{F}_1(ę)}(x̧), 1 - I_{\tilde{F}_2(ę)}(x̧)\}, \\ F_{\tilde{F}3(e)}(x̧) = max\{F_{\tilde{F}_1(ę)}(x̧), T_{\tilde{F}_2(ę)}(x̧)\}. \end{cases}$$

Definition 2.7 [32] I: A NSS $(\widetilde{F_1}, É)$ is said to be null NSS if$T_{\tilde{F}(ę)}(x̧) = 0, I_{\tilde{F}(ę)}(x̧) = 0, F_{\tilde{F}(ę)}(x̧) = 1 : ∀ę \in É, ∀x̧ \in Ũ$. It is denoted by $0_{(Ũ,É)}$.

2. A NSS $(\widetilde{F_1}, É)$ is said to be absolute NSS if$T_{\tilde{F}(ę)}(x̧) = 1, I_{\tilde{F}(ę)}(x̧) = 1, F_{\tilde{F}(ę)}(x̧) = 0; ∀x̧ \in Ũ, ∀ę \in É$. It is symbolized as$1_{(Ũ,É)}$.

$1^c_{(Ũ,É)} = 0_{(Ũ,É)} =, 0^c_{(Ũ,É)} = 1_{(Ũ,É)}$ is obvious.

3. Basic of quadri-partitioned neutrosophic soft sets

Definition 3.1 [33] É represents a collection of parameters, and Ũ denotes an initial universe set. $P(Ũ)$ denotes the set of all NSs for Ũ. A set defined by a set valued function $F̃$ that represents a mapping of the form $F̃ : É \to P(Ũ)$ is called QPNSS $(\tilde{F}, É)$ over Ũ, with $\tilde{F}$ being the approximate function of this NSS. In other terms, the QPNSS can be described as a set of ordered pairs, $(\tilde{F}, É) = \left[\left(ę, \langle x̧, ÆbT_{\tilde{F}(ę)^{(x̧)}}, ŖęT_{\tilde{F}(ę)^{(x̧)}}, ŖęF_{\tilde{F}(ę)^{(x̧)}}, ÆbF_{\tilde{F}(ę)^{(x̧)}} : x̧ \in Ũ\rangle\right) : ę \in É\right]$with $ŧÆbT_{\tilde{F}(ę)^{(x̧)}}, ŖęT_{\tilde{F}(ę)^{(x̧)}}, ŖęF_{\tilde{F}(ę)^{(x̧)}}, ÆbF_{\tilde{F}(ę)^{(x̧)}} \in [0,1]$ are, called the absolute true, relative true, relative false, *and absolute false- membership functions* of $\tilde{F}$ (ę) and all of which lie within the interval [0,1] with $0 \leq ÆbT_{\tilde{F}(ę)^{(x̧)}} + ŖęT_{\tilde{F}(ę)^{(x̧)}} + ŖęF_{\tilde{F}(ę)^{(x̧)}} + ÆbF_{\tilde{F}(ę)^{(x̧)}} \leq 4$ is clear since the supremum of each is 1.

Definition 3.2 [33] The complement of QPNSS $(\tilde{F}, É)$is denoted by $(\tilde{F}, É)^c$ and is given as :

$(\tilde{F}, É)^c = \left[\left(ę, \langle x̧, ÆbF_{\tilde{F}(ę)^{(x̧)}}, ŖęF_{\tilde{F}(ę)^{(x̧)}}, ŖęT_{\tilde{F}(ę)^{(x̧)}}, ÆbT_{\tilde{F}(ę)^{(x̧)}} : x̧ \in Ũ\rangle\right) : ę \in É\right], \left((\tilde{F}, É)^c\right)^c = (\tilde{F}, É).$

Definition 3.3 [33] $(\tilde{F}, É)$ is sub set of $(\tilde{G}, É)$ if $ÆbT_{\tilde{F}(ę)^{(x̧)}} \preccurlyeq ÆbT_{G(ę)^{(x̧)}}, ŖęT_{\tilde{F}(ę)^{(x̧)}} \preccurlyeq ReT_{\tilde{G}(ę)^{(x̧)}}, ŖęF_{\tilde{F}(ę)^{(x̧)}} \succcurlyeq ŖęF_{\tilde{G}(ę)^{(x̧)}}, ÆbF_{\tilde{F}(ę)^{(x̧)}} \succcurlyeq ÆbF_{\tilde{G}(ę)^{(x̧)}}, ∀ ę \in É$ *and* $∀ x̧ \in Ũ$.

Definition 3.4 [33] The union of two QPNSSs $(\tilde{F}, É), (\tilde{G}, É)$ is given as $(\tilde{F}, É)\tilde{U}(\tilde{G}, É) = (\tilde{H}, É)$ with $(\tilde{H}, É) = \left[\left(ę, \langle x̧, ÆbT_{\tilde{H}(ę)^{(x̧)}}, ŖęT_{\tilde{H}(ę)^{(x̧)}}, ŖęF_{\tilde{H}(ę)^{(x̧)}}, ÆbF_{L(ę)^{(x̧)}} : x̧ \in Ũ\rangle\right) : ę \in É\right]$

With $\text{Ab}T_{\tilde{H}(ę)^{(x)}} = \text{m}\dot{a}x\left[\text{Ab}T_{\tilde{F}(ę)^{(x)}}, \text{Ab}T_{G(ę)^{(x)}}\right]$, $\text{Re}T_{\tilde{H}(ę)^{(x)}} = \text{m}\dot{a}x\left[\text{Re}T_{\tilde{F}(ę)^{(x)}}, \text{Re}T_{G(ę)^{(x)}}\right]$,

$\text{Re}F_{\tilde{H}(ę)^{(x)}} = \text{m}\dot{i}n\left[\text{Re}F_{\tilde{F}(ę)^{(x)}}, \text{Re}F_{G(ę)^{(x)}}\right]$, $F_{\tilde{H}(ę)^{(x)}} = \text{m}\dot{i}n\left[\text{Ab}F_{\tilde{F}(ę)^{(x)}}, \text{Ab}F_{G(ę)^{(x)}}\right]$.

Definition 3.5 [33] The intersection of QPNSSs $(\tilde{F}, \acute{E}), (\tilde{G}, \acute{E})$ is denoted by $(\tilde{F}, \acute{E})\tilde{\cap}(\tilde{G}, \acute{E}) = (\tilde{H}, \acute{E})$and is given as

$$(\tilde{H}, \acute{E}) = \left[\left(ę, \langle x, \text{Ab}T_{\tilde{H}(ę)^{(x)}}, \text{Re}T_{\tilde{H}(ę)^{(x)}}, \text{Re}F_{\tilde{H}(ę)^{(x)}}, \text{Ab}F_{L(ę)^{(x)}} : x \in \tilde{U}\rangle\right) : ę \in \acute{E}\right]$$

Where, $\text{Ab}T_{\tilde{H}(ę)^{(x)}} = \text{m}\dot{a}x\left[\text{Ab}T_{\tilde{F}(ę)^{(x)}}, \text{Ab}T_{G(ę)^{(x)}}\right]$, $\text{Re}T_{\tilde{H}(ę)^{(x)}} = \text{m}\dot{i}n\left[\text{Re}T_{\tilde{F}(ę)^{(x)}}, \text{Re}T_{G(ę)^{(x)}}\right]$,

$$\text{Re}F_{\tilde{H}(ę)^{(x)}} = \text{m}\dot{a}x\left[\text{Re}F_{\tilde{F}(ę)^{(x)}}, \text{Re}F_{G(ę)^{(x)}}\right], \; F_{\tilde{H}(ę)^{(x)}} = \text{m}\dot{a}x\left[\text{Ab}F_{\tilde{F}(ę)^{(x)}}, \text{Ab}F_{G(ę)^{(x)}}\right].$$

Definition 3.6 [33] The difference of two QPNSSs $(\tilde{F}, \acute{E}), (\tilde{G}, \acute{E})$ *is* $(\tilde{H}, \acute{E}) = (\tilde{F}, \acute{E})\tilde{\cap}(\tilde{G}, \acute{E})^{c}$ *and* is given as $(\tilde{H}, \acute{E}) = \left[\left(ę, \langle x, \text{Ab}T_{\tilde{H}(ę)^{(x)}}, \text{Re}T_{\tilde{H}(ę)^{(x)}}, \text{Re}F_{\tilde{H}(ę)^{(x)}}, \text{Ab}F_{L(ę)^{(x)}} : x \in \tilde{U}\rangle\right) : ę \in \acute{E}\right]$ with $\text{Ab}T_{\tilde{H}(ę)^{(x)}} = \text{m}\dot{i}n\left[\text{Ab}T_{\tilde{F}(ę)^{(x)}}, \text{Ab}F_{G(ę)^{(x)}}\right]$, $\text{Re}T_{\tilde{H}(ę)^{(x)}} = \text{m}\dot{i}n\left[\text{Re}T_{\tilde{F}(ę)^{(x)}}, \text{Re}F_{G(ę)^{(x)}}\right]$,

$$\text{Re}F_{\tilde{H}(ę)^{(x)}} = \text{m}\dot{a}x\left[\text{Re}F_{\tilde{F}(ę)^{(x)}}, \text{Re}T_{G(ę)^{(x)}}\right], \; F_{\tilde{H}(ę)^{(x)}} = \text{m}\dot{a}x\left[\text{Ab}F_{\tilde{F}(ę)^{(x)}}, \text{Ab}F_{G(ę)^{(x)}}\right].$$

Definition 3.7 [33] The family of all QPNSSs is $\text{QNSS}\left(\tilde{U}, \acute{E}\right)$. If $\tau \subset \text{QPNSS}\left(\tilde{U}, \acute{E}\right)$, then$\tau$ is QPNSTS on $\tilde{U}$ if(1).$0_{(\langle \tilde{U}\rangle, \acute{E})}, 1_{(\langle \tilde{U}\rangle, \acute{E})} \in \tau$, (2).The union of any number of $QPNSSs$ in $\tau \in \tau$.

(3).*T*he intersection of a fi*n*ite number of $QPNSSs\ in\ \tau \in \tau$, then $(\tilde{U}, \tau, \acute{E})$ is QPNSTTS over $\tilde{U}$.

4. P- Compactness in quadri-partitioned neutrosophic topological spaces (QPNSBTS)

The notion of QPNS compactness in QPNSBTS and QPNS p-compact space is covered in this section. We define and discuss the notion of reducibility to finite sub-covers, which is one of the features of a QPNS cover. A number of intriguing theorems demonstrate that a QPNS p-compact space possesses the finite intersection property of its QPNS p-closed sets and that the intersection of QPNS p-closed sets is non-empty. We further prove that a QPNS p-closed subspace of a QPNS p-compact space is QPNS p-compact and that non-overlapping QPNS p-open subsets exist that divide disjoint QPNS p-compact subsets of a QPNS p-Hausdorff space. This contribution has improved the theoretical underpinnings of the QPNS spaces and has proven helpful in the research of compactness in the soft topological spaces.

Definition 4.1 Let $(\tilde{U}, \tau_1, \tau_2, \acute{E})$ be a QPNSBTS $over\ \tilde{U}$, $(\tilde{\tilde{Y}}, \acute{E})be\ a\ QPNSS$, then $(\tilde{\tilde{Y}}, \acute{E})$ is (1): $QPNS$ s-open if $QPNScl\left(QPNSint(\tilde{\tilde{Y}}, \acute{E})\right) \cong (\tilde{\tilde{Y}}, \acute{E})$

(2): $QPNSBTS\ p\text{-}open$) if $QPNS\text{int}\left(QPNScl(\tilde{\tilde{Y}}, \acute{E})\right) \cong (\tilde{\tilde{Y}}, \acute{E})$

Definition 4.2 The class of sub-set of $\tilde{U}$ is $(\tilde{\mathcal{O}}, \acute{E}) = \{(\tilde{\mathcal{O}}, \acute{E})_i\}$. If $(\tilde{\mathcal{L}}, \acute{E}) \tilde{\subseteq} \tilde{U}$ if $(\tilde{\mathcal{L}}, \acute{E}) \tilde{\subseteq} U(\tilde{\mathcal{O}}, \acute{E})_i$. The class $\{(\tilde{\mathcal{O}}, \acute{E})_i\}$ is referred to be QPNScover of $(\tilde{\mathcal{L}}, \acute{E})$. Since members of the aforementioned class are finite, countable, and QPNS p-open, this cover is referred to as finite, countable, and QPNS

p-open according as the members of the above class are finite, countable and QPNS p-open. (i) $\left(\widetilde{\mathfrak{L}}, \acute{\mathrm{E}}\right)_1 = (\widetilde{\mathfrak{F}}, \acute{\mathrm{E}})_1 \mathrm{U} (\widetilde{\mathfrak{F}}, \acute{\mathrm{E}})_2 \mathrm{U} (\widetilde{\mathfrak{F}}, \acute{\mathrm{E}})_3$

(ii) if $\left(\widetilde{\mathfrak{L}}, \acute{\mathrm{E}}\right)_1 = \{(\widetilde{\mathfrak{F}}, \acute{\mathrm{E}})_i : i \cong I\}$

$\left(\widetilde{\mathfrak{L}}, \acute{\mathrm{E}}\right)_2 = \{(\tilde{\mathrm{L}}, \acute{\mathrm{E}})_j : j \cong I\}$ are two QPNS cover of a set $\left(\widetilde{\mathfrak{L}}, \acute{\mathrm{E}}\right)$

i.e. $\left(\widetilde{\mathfrak{L}}, \acute{\mathrm{E}}\right) \cong \mathrm{U}(\widetilde{\mathfrak{F}}, \acute{\mathrm{E}})_i$ and $\left(\widetilde{\mathfrak{L}}, \acute{\mathrm{E}}\right) \cong \mathrm{U}(\tilde{\mathrm{L}}, \acute{\mathrm{E}})_j$ so that candidate of $\left(\widetilde{\mathfrak{L}}, \acute{\mathrm{E}}\right)_2$ is also candidate of $\left(\widetilde{\mathfrak{L}}, \acute{\mathrm{E}}\right)_1$. Then $\left(\widetilde{\mathfrak{L}}, \acute{\mathrm{E}}\right)_2$ is referred to be QPNS sub-cover of $\left(\widetilde{\mathfrak{L}}, \acute{\mathrm{E}}\right)_1$

Definition 4.3 If $\left(\widetilde{\mathfrak{L}}, \acute{\mathrm{E}}\right)) = \left\{\left(\widetilde{\mathfrak{F}}, \acute{\mathrm{E}}\right)_i : i \cong I\right\}$ is a class of QPNS and $\left(\widetilde{\mathfrak{L}}, \acute{\mathrm{E}}\right) \cong \tilde{\mathrm{U}}$ $s.t.$ $\left(\widetilde{\mathfrak{L}}, \acute{\mathrm{E}}\right) \cong \mathrm{U}(\widetilde{\mathfrak{F}}, \acute{\mathrm{E}})_i$ then $\left(\widetilde{\mathfrak{L}}, \acute{\mathrm{E}}\right) = \{(\widetilde{\mathfrak{F}}, \acute{\mathrm{E}})_i : i \cong I\}$ is a QPNS p-cover. If $(\widetilde{\mathfrak{F}}, \acute{\mathrm{E}})_{i_1}, (\widetilde{\mathfrak{F}}, \acute{\mathrm{E}})_{i_2}, (\widetilde{\mathfrak{F}}, \acute{\mathrm{E}})_{i_3}, \ldots . (\widetilde{\mathfrak{F}}, \acute{\mathrm{E}})_{i_k}$ are from $\left(\widetilde{\mathfrak{L}}, \acute{\mathrm{E}}\right)$ s.t. $\left(\widetilde{\mathfrak{L}}, \acute{\mathrm{E}}\right) \cong (\widetilde{\mathfrak{F}}, \acute{\mathrm{E}})_{i_1} \mathrm{U} (\widetilde{\mathfrak{F}}, \acute{\mathrm{E}})_{i_2} \mathrm{U} (\widetilde{\mathfrak{F}}, \acute{\mathrm{E}})_{i_3}, \ldots . \mathrm{U} (\widetilde{\mathfrak{F}}, \acute{\mathrm{E}})_{i_k}$ or $\left(\widetilde{\mathfrak{L}}, \acute{\mathrm{E}}\right) \cong \mathrm{U}_{n=1}^{k} (\widetilde{\mathfrak{F}}, \acute{\mathrm{E}})_{ik}$. Then $\left(\widetilde{\mathfrak{L}}, \acute{\mathrm{E}}\right) = \{(\widetilde{\mathfrak{F}}, \acute{\mathrm{E}})_i : i \cong I\}$ can be shrunk to finite sun-cover.

Definition 4.4 If $(\tilde{\mathrm{U}}, \tau_1, \tau_2, \acute{\mathrm{E}})$ be a QPNSBTS over $\tilde{\mathrm{U}}$and $\left(\widetilde{\mathfrak{L}}, \acute{\mathrm{E}}\right) \cong \tilde{\mathrm{U}})$ then this set $\left(\widetilde{\mathfrak{L}}, \acute{\mathrm{E}}\right)$is compact if every QPNS p-open covering of $\left(\widetilde{\mathfrak{L}}, \acute{\mathrm{E}}\right)$ can be reduced to FSC .

Definition 4.5 If $\widetilde{\tilde{\mathrm{U}}}$ isQPNS. The collection ofQPNS sub-sets of $\widetilde{\tilde{\mathrm{U}}}$ say $\left\{\left(\widetilde{\mathfrak{L}}, \acute{\mathrm{E}}\right)_\alpha : \alpha \in I\right\}$ have FIP if we can search out soft QPNS (finite) sub-collection

$\{\left(\widetilde{\mathfrak{L}}, \acute{\mathrm{E}}\right)_{\alpha_1}, \left(\widetilde{\mathfrak{L}}, \acute{\mathrm{E}}\right)_{\alpha_2}, \left(\widetilde{\mathfrak{L}}, \acute{\mathrm{E}}\right)_{\alpha_3} \ldots \ldots \ldots . \left(\widetilde{\mathfrak{L}}, \acute{\mathrm{E}}\right)_{\alpha_n}\}$ $s.t$

$$\left(\widetilde{\mathfrak{L}}, \acute{\mathrm{E}}\right)_{\alpha_1} \tilde{\cap} \left(\widetilde{\mathfrak{L}}, \acute{\mathrm{E}}\right)_{\alpha_2} \tilde{\cap} \left(\widetilde{\mathfrak{L}}, \acute{\mathrm{E}}\right)_{\alpha_3} \tilde{\cap} \ldots \ldots \ldots . \tilde{\cap} \left(\widetilde{\mathfrak{L}}, \acute{\mathrm{E}}\right)_{\alpha_n} \ncong \tilde{\Phi}$$

or $\prod_{i=1}^{n} \left(\widetilde{\mathfrak{L}}, \acute{\mathrm{E}}\right)_{\alpha_i} \ncong \tilde{\Phi}$.

Theorem 4.6 Assume that each class of QPNS p-closed sets with finite intersection property has a non-empty intersection if and only if $(\widetilde{\tilde{\mathrm{U}}}, \tau_1, \tau_2, \acute{\mathrm{E}})$ is QPNS p-compact.

Proof. Assume that $(\widetilde{\tilde{\mathrm{U}}}, \tau_1, \tau_2, \acute{\mathrm{E}})$ is QPNS p-compact and $\left\{\left(\widetilde{\mathfrak{L}}, \acute{\mathrm{E}}\right)_\alpha : \alpha \in I\right\}$ be a class of QPNS p-CSs satisfying FIP that is $\prod_{i=1}^{n} \left(\widetilde{\mathfrak{L}}, \acute{\mathrm{E}}\right)_{\alpha_i} \ncong \tilde{\Phi}$. If $\prod_{i=1}^{n} \left(\widetilde{\mathfrak{L}}, \acute{\mathrm{E}}\right)_{\alpha_i} \cong \tilde{\Phi} \Longrightarrow (\prod_{i=1}^{n} \left(\widetilde{\mathfrak{L}}, \acute{\mathrm{E}}\right)_{\alpha_i})^c \cong \Phi^c$. this implies that $(\coprod_{i}^{n} \left(\widetilde{\mathfrak{L}}, \acute{\mathrm{E}}\right)_{\alpha_i})^c \cong \Phi^c$. Implies$\tilde{\tilde{\mathrm{U}}} \cong (\coprod_{i}^{n} \left(\widetilde{\mathfrak{L}}, \acute{\mathrm{E}}\right)_{\alpha_i})^c$. This means $\left\{\left(\widetilde{\mathfrak{L}}, \acute{\mathrm{E}}\right)_\alpha : \alpha \in I\right\} \cong \{\left(\widetilde{\mathfrak{L}}, \acute{\mathrm{E}}\right)_1^{\ c}, \left(\widetilde{\mathfrak{L}}, \acute{\mathrm{E}}\right)_2^{\ c}, \left(\widetilde{\mathfrak{L}}, \acute{\mathrm{E}}\right)_3^{\ c} \ldots\}$ forms QPNS p-OC of $\tilde{\mathrm{U}}$. But $\left(\widetilde{\tilde{\mathrm{U}}}, \tau_1, \tau_2, \acute{\mathrm{E}}\right)$ is QPNS p-compact. So $\tilde{\mathrm{U}} \cong \coprod_{k \cong \tilde{1}}^{n} \left(\widetilde{\mathfrak{L}}, \acute{\mathrm{E}}\right)_{i_k})^c$. This implies $(\prod_{i=1}^{n} \widetilde{\mathfrak{L}}, \acute{\mathrm{E}}_{i_i})^c \cong \tilde{\tilde{\mathrm{U}}}^c$. Implies $\left[\left(\prod_{k=1}^{n} \left(\widetilde{\mathfrak{L}}, \acute{\mathrm{E}}\right)_{i_k}\right)^c\right]^c \cong \tilde{\Phi}$. This implies$\prod_{k=\tilde{1}}^{n} \left(\widetilde{\mathfrak{L}}, \acute{\mathrm{E}}\right)_{i_k}) \cong \tilde{\Phi}$ which is not possible. Hence$\prod_{i=1}^{n} \left(\widetilde{\mathfrak{L}}, \acute{\mathrm{E}}\right)_{\alpha_i} \ncong \tilde{\Phi}$. On converse we are prove is QPNS p-compact. If not QPNS p-compact. Implies least one QPNS p-OC is there which is not reducible to FSC. Let that QPNS p-OC be $\left\{\left(\widetilde{\mathfrak{F}}, \acute{\mathrm{E}}\right)_i : i \in I\right\}$. Since this is QPNS p-open cover of $\tilde{\mathrm{U}}$. So $\tilde{\mathrm{U}} \cong \coprod_{i \in I} \left(\widetilde{\mathfrak{L}}, \acute{\mathrm{E}}\right)_i$ .But$\tilde{\mathrm{U}} \ncong \coprod_{k \cong \tilde{1}}^{\tilde{m}} \left(\widetilde{\mathfrak{F}}, \acute{\mathrm{E}}\right)_{i_k}$. This implies$\prod_{k=\tilde{1}}^{\tilde{m}} \left(\widetilde{\mathfrak{F}}, \acute{\mathrm{E}}\right)_{ik}^{\ c} \ncong \tilde{\Phi}$. Where $\left(\widetilde{\mathfrak{F}}, \acute{\mathrm{E}}\right)_{ik}^{\ c}$ are soft p-closed. But $\prod_{i \in I} \left(\widetilde{\mathfrak{F}}, \acute{\mathrm{E}}\right)_i^{\ c} \ncong \tilde{\Phi}$. This implies $\tilde{\mathrm{U}} \ncong \tilde{\coprod}_{i \in I} (\widetilde{\mathfrak{F}}, \acute{\mathrm{E}})_i$ which is possible. Hence $\tilde{\mathrm{U}}$ is QPNS p-compact.

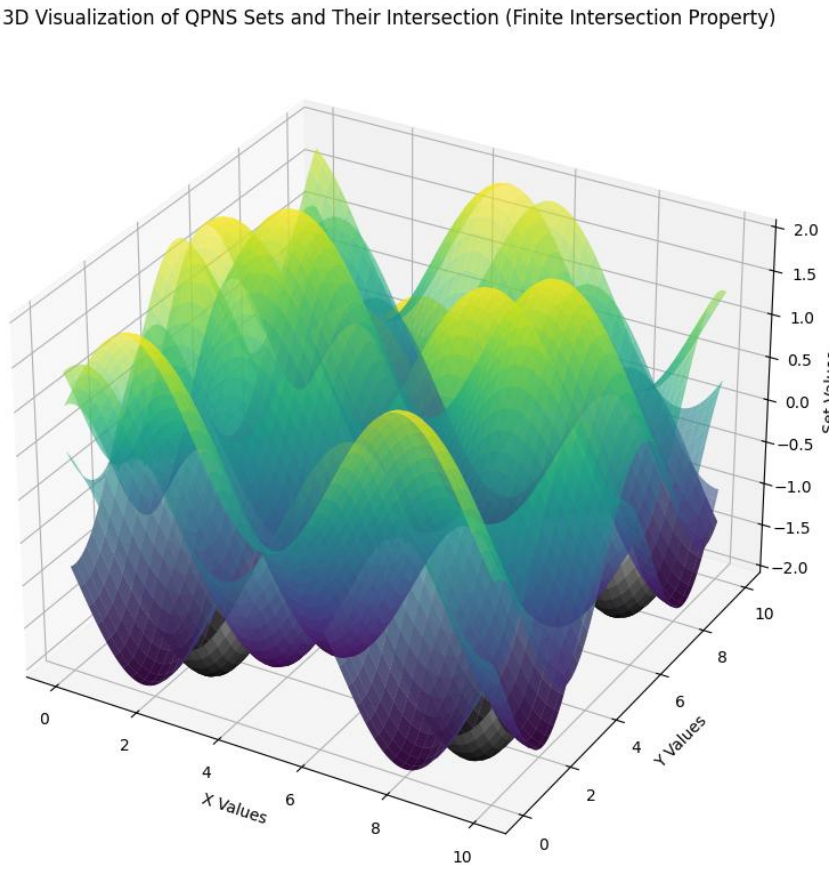
3D Visualization of QPNS Sets and Their Intersection (Finite Intersection Property)
X Values
Y Values
Set Value
0
2
4
6
8
10
2.0
1.5
1.0
0.5
0.0
−0.5
−1.0
−1.5
−2.0

Fig: 4.1

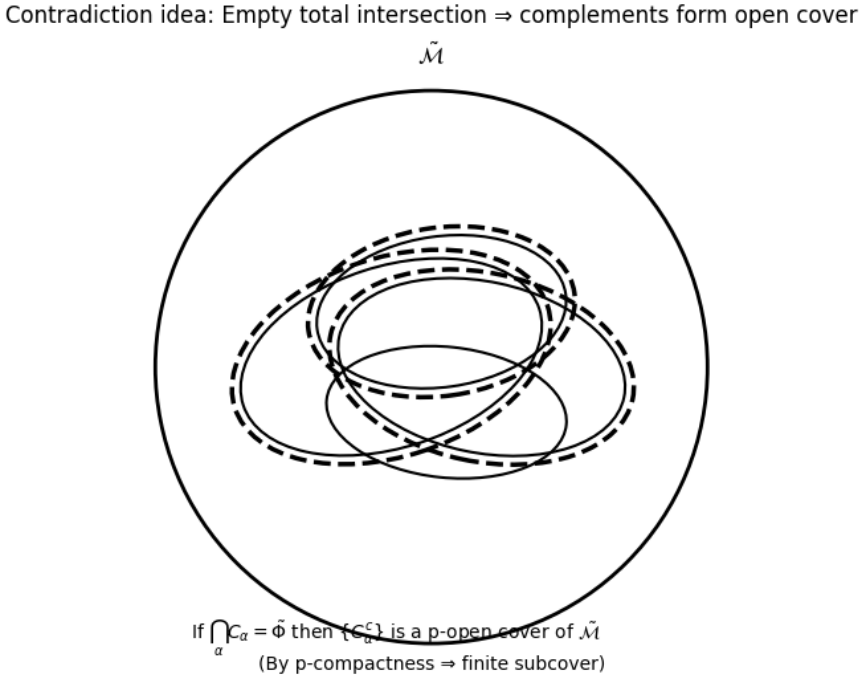
Contradiction idea: Empty total intersection ⇒ complements form open cover
$\tilde{\mathcal{M}}$
If $\bigcap_{\alpha} C_\alpha = \tilde{\Phi}$ then $\{C_\alpha^c\}$ is a p-open cover of $\tilde{\mathcal{M}}$
(By p-compactness ⇒ finite subcover)

Fig: 4.2

Theorem 4.7 If $(\widetilde{\tilde{U}}, \tau_1, \tau_2, É)$ is QPNSTS, p-CSS of a QPNS p-CS is QPNS p-compact.

Proof. Assume $(\widetilde{\tilde{U}}, \tau_1, \tau_2, É)$ is QPNSTS $s.t.$ it is QPNS p-compact, $(\tilde{Ḉ}, É)$ is a QPNS p-CSS. Let $\left\{(\tilde{ð}, É)_i : i \in I\right\}$ be QPNS p-OC of $(\tilde{Ḉ}, É)$. Since $\left\{(\tilde{ð}, É)_i : i \in I\right\}$is QPNS p-*open cover of* $(\tilde{Ḉ}, É)$ so $(\tilde{Ḉ}, É) \tilde{\subseteq} \coprod_{i\in I}(\tilde{\tilde{ð}}, É)_i$. Now $\tilde{U} \cong (\tilde{Ḉ}, É) \cup (\tilde{Ḉ}, É)^c$.Now $(\tilde{Ḉ}, É) \cup (\tilde{Ḉ}, É)^c \tilde{\subseteq} \coprod_{i\in I}(\tilde{\tilde{ð}}, É)_i \cup (\tilde{Ḉ}, É)^c$.$\tilde{U} \cong (\coprod_{i\in I}(\tilde{\tilde{ð}}, É)_i) \cup (\tilde{Ḉ}, É)^c$. Since $(\tilde{Ḉ}, É)$ is QPNS p-closed this implies $(\tilde{Ḉ}, É)^c$ is QPNS p-open.

The soft family $\left\{(\tilde{ð}, É)_i : i \in I\right\}$ together with $(\tilde{Ḉ}, É)^c$ form QPNS p-open cover of$\tilde{U}$. But $\tilde{U}$ is given to be QPNS p-compact. So the above QPNS p-OC can be reduced to finite QPNS sub-cover. That is$\tilde{U} \cong (\coprod_{k\tilde{\cong}\tilde{1}}^{n}(\tilde{ð}, É)_{i_k}) \cup (\tilde{Ḉ}, É)^c$. This implies $(\tilde{Ḉ}, É) \tilde{\subseteq} (\coprod_{k\tilde{\cong}\tilde{1}}^{n}(\tilde{ð}, É)_{i_k}) \cup (\tilde{Ḉ}, É)^c$. But$(\tilde{Ḉ}, É) \tilde{\cap} (\tilde{Ḉ}, É)^c \cong \tilde{\Phi}$. So$(\tilde{Ḉ}, É) \tilde{\subseteq} (\coprod_{k\tilde{\cong}\tilde{1}}^{n}(\tilde{ð}, É)_{i_k})$.This implies $\left\{(\tilde{ð}, É)_i : i \in I\right\}$ which QPNS p-open cover is of $(\tilde{Ḉ}, É)$ is reduced to finite QPNS sub-cover. So $(\tilde{Ḉ}, É)$is QPNS p-compact.

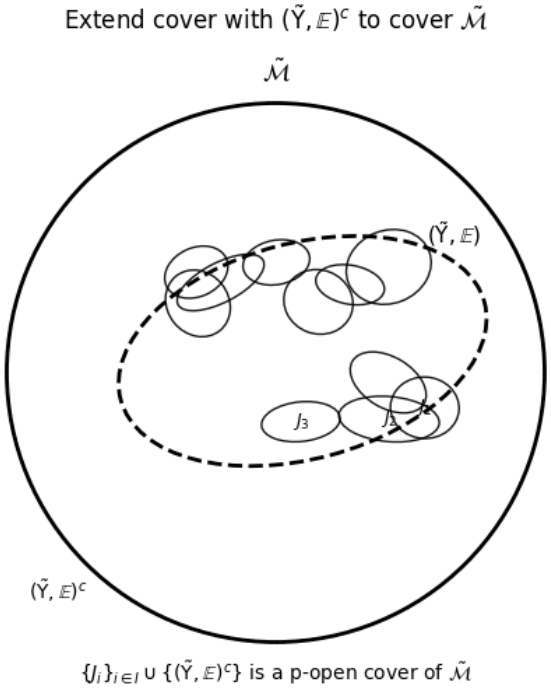

Fig: 4.3

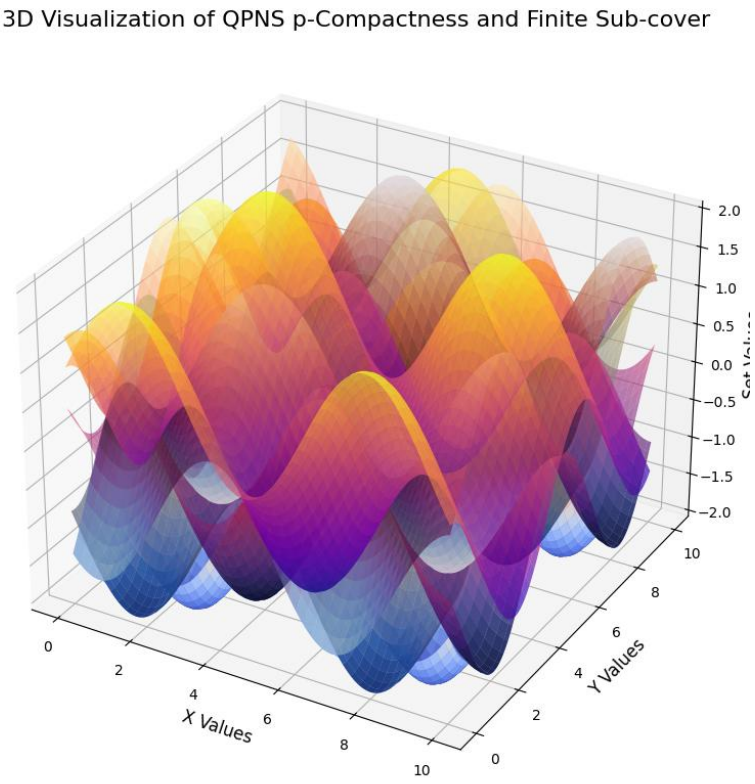

Fig: 4.4

Theorem 4.8 Assume QPNS p-Hausdorff space $\tilde{U}$. If $(\tilde{\mathcal{L}}, \acute{E})$ is QPNS p-compact SS and let $\S^{\wedge}_{\langle p_1,p_2,p_3,p_4\rangle} \in \tilde{U} - (\tilde{\mathcal{L}}, \acute{E})$. *Then there exists* QPNS p-OS $(\tilde{\mathcal{O}}, \acute{E})$ and $(\tilde{L}, \acute{E})$ s.t. $\S^{\wedge}_{\langle p_1,p_2,p_3,p_4\rangle} \in (\tilde{\mathcal{O}}, \acute{E})$, $(\tilde{\mathcal{L}}, \acute{E}) \tilde{\subseteq} (\tilde{L}, \acute{E})$ and $(\tilde{\mathcal{O}}, \acute{E}) \tilde{\cap} (\tilde{L}, \acute{E}) \cong \tilde{\Phi}$.

Proof. $\tilde{U}$ is given to be QPNS p-Hausdorff space, for each $\S^{\wedge}_{\langle p_1,p_2,p_3,p_4\rangle} \in (\tilde{\mathcal{L}}, \acute{E})$ there exists QPNS p-Oss $(\tilde{\mathcal{O}}_{\S^{\wedge}_{\langle p_1,p_2,p_3,p_4\rangle}}, \acute{E})$ and $(\tilde{L}_{\S^{\wedge}_{\langle p_1,p_2,p_3,p_4\rangle}}, \acute{E})$ respectively such that $\left(\tilde{\mathcal{O}}_{\S^{\wedge}_{\langle p_1,p_2,p_3,p_4\rangle}}, \acute{E}\right) \tilde{\cap} (\tilde{L}_{\S^{\wedge}_{\langle p_1,p_2,p_3,p_4\rangle}}, \acute{E}) \cong \tilde{\Phi}$. Now $\{(\tilde{L}_{\tilde{x}}, \acute{E}): \S^{\wedge}_{\langle p_1,p_2,p_3,p_4\rangle} \in (\tilde{\mathcal{L}}, \acute{E})\}$ is QPNS p-OC of $(\tilde{\mathcal{L}}, \acute{E})$ and $(\tilde{\mathcal{L}}, \acute{E})$ being QPNS p-*c*ompact, there exists finitely many points of $\S_1{}^{\wedge}_{\langle p_1,p_2,p_3,p_4\rangle}, \S_2{}^{\wedge}_{\langle p_1,p_2,p_3,p_4\rangle}, \S_3{}^{\wedge}_{\langle p_1,p_2,p_3,p_4\rangle}, \S_4{}^{\wedge}_{\langle p_1,p_2,p_3,p_4\rangle}, \dots\dots\dots \S_n{}^{\wedge}_{\langle p_1,p_2,p_3,p_4\rangle}$ of $(\tilde{\mathcal{L}}, \acute{E})$ such that$(\tilde{\mathcal{L}}, \acute{E}) \tilde{\subseteq} \tilde{\cup}_{i=1}^{n} \left(\tilde{L}_{\S_i{}^{\wedge}_{\langle p_1,p_2,p_3,p_4\rangle}}, \acute{E}\right)$. Let $(\tilde{L}, \acute{E}) \cong \tilde{\cup}_{i=1}^{n} \left(\tilde{L}_{\S_i{}^{\wedge}_{\langle p_1,p_2,p_3,p_4\rangle}}, \acute{E}\right)$ and$(\tilde{\mathcal{O}}, \acute{E}) \cong \tilde{\cap}_{i=1}^{n} (\tilde{\mathcal{O}}_{\S_i{}^{\wedge}_{\langle p_1,p_2,p_3,p_4\rangle}}, \acute{E})$. Then $(\tilde{L}, \acute{E})$ and $(\tilde{\mathcal{O}}, \acute{E})$ *are clearly* QPNS p-OSs *s.t.* $\S^{\wedge}_{\langle p_1,p_2,p_3,p_4\rangle} \in (\tilde{\mathcal{O}}, \acute{E}) \tilde{\subseteq} (\tilde{L}, \acute{E})$. More over$(\tilde{\mathcal{O}}, \acute{E}) \tilde{\cap} (\tilde{L}, \acute{E}) \cong \tilde{\Phi}$, ify$^{\wedge}_{\langle p_1,p_2,p_3,p_4\rangle} \in (\tilde{L}, \acute{E})$, then if $y^{\wedge}_{\langle p_1,p_2,p_3,p_4\rangle} \in (\tilde{L}, \acute{E})$ implies that $y^{\wedge}_{\langle p_1,p_2,p_3,p_4\rangle} \in \left(\tilde{L}_{\S_i{}^{\wedge}_{\langle p_1,p_2,p_3,p_4\rangle}}, \acute{E}\right)$ for some $\S_i{}^{\wedge}_{\langle p_1,p_2,p_3,p_4\rangle}$impliesy$^{\wedge}_{\langle p_1,p_2,p_3,p_4\rangle} \notin (\tilde{\mathcal{O}}_{\S_i{}^{\wedge}_{\langle p_1,p_2,p_3,p_4\rangle}}, \acute{E})$. Since $(\tilde{\mathcal{O}}_{\S^{\wedge}_{\langle p_1,p_2,p_3,p_4\rangle}}, \acute{E}) \tilde{\cap} (\tilde{L}_{\S^{\wedge}_{\langle p_1,p_2,p_3,p_4\rangle}}, \acute{E}) \cong \tilde{\Phi}$ implies $y^{\wedge}_{\langle p_1,p_2,p_3,p_4\rangle} \notin \tilde{\cap}_{i=1}^{n} (\tilde{\mathcal{O}}_{\S_i{}^{\wedge}_{\langle p_1,p_2,p_3,p_4\rangle}}, \acute{E})$ impliesy$^{\wedge}_{\langle p_1,p_2,p_3,p_4\rangle} \notin (\tilde{\mathcal{O}}, \acute{E})$.

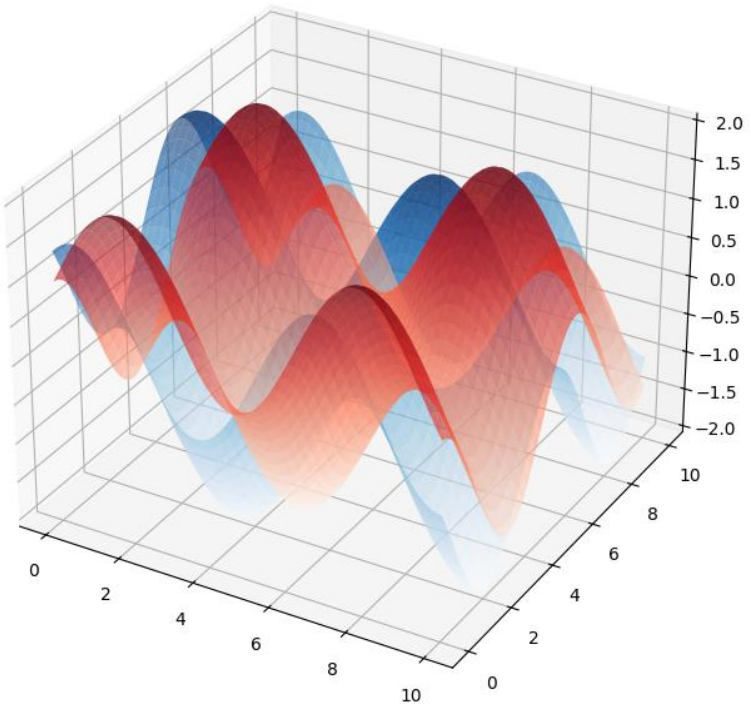
2.0
1.5
1.0
0.5
0.0
−0.5
−1.0
−1.5
−2.0
0
2
4
6
8
10
0
2
4
6
8
10

Fig: 4.5

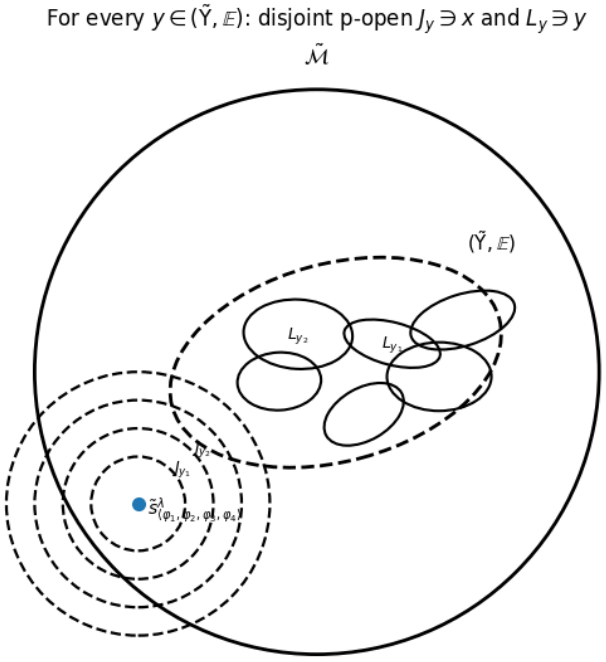
For every $y \in (\tilde{Y}, \mathbb{E})$: disjoint p-open $J_y \ni x$ and $L_y \ni y$
$\tilde{\mathcal{M}}$
$(\tilde{Y}, \mathbb{E})$
L_{y_2}
L_{y_3}
J_{y_2}
J_{y_1}
$\tilde{S}^{\lambda}_{(\varphi_1, \varphi_2, \varphi_3, \varphi_4)}$

Fig: 4.6

Theorem 4.9 Let $(\tilde{\mathfrak{L}}, \acute{E})$ and $(\tilde{\varpi}, \acute{E})$ be dis-joint QPNS p-compact SSs of a QPNS p-Hausdorff of $\tilde{U}$. Then, there exists disjoint QPNS p-Oss $(\tilde{\mathfrak{F}}, \acute{E})$ and $(\tilde{L}, \acute{E})$ $s.t.,(\tilde{\mathfrak{L}}, \acute{E}) \tilde{\subseteq} (\tilde{\mathfrak{F}}, \acute{E})$and $(\tilde{\varpi}, \acute{E}) \tilde{\subseteq} (\tilde{L}, \acute{E})$.

Proof. $\dot{s}^{\wedge}_{\langle p_1,p_2,p_3,p_4\rangle} \in (\tilde{\mathfrak{L}}, \acute{E})$. Since$(\tilde{\mathfrak{L}}, \acute{E}) \tilde{\cap} (\tilde{\mathfrak{F}}, \acute{E}) \cong \tilde{\Phi}$, $y^{\wedge}_{\langle p_1,p_2,p_3,p_4\rangle} \notin (\tilde{\mathfrak{F}}, \acute{E})$; Now, $(\tilde{\varpi}, \acute{E})$ is a QPNS p-compact SS of a QPNS p-Hausdorff of $\tilde{U}$ and $\dot{s}^{\wedge}_{\langle p_1,p_2,p_3,p_4\rangle} \notin (\tilde{\varpi}, \acute{E})$, so there exists QPNS p-OSs $(\tilde{\mathfrak{F}}_{\dot{s}^{\wedge}_{\langle p_1,p_2,p_3,p_4\rangle}}, \acute{E})$ and $(\tilde{L}_{\dot{s}^{\wedge}_{\langle p_1,p_2,p_3,p_4\rangle}}, \acute{E})$ such that $\dot{s}^{\wedge}_{\langle p_1,p_2,p_3,p_4\rangle} \in (\tilde{\mathfrak{F}}_{\dot{s}^{\wedge}_{\langle p_1,p_2,p_3,p_4\rangle}}, \acute{E}), (\tilde{\mathfrak{F}}, \acute{E}) \tilde{\subseteq} (\tilde{L}_{\dot{s}^{\wedge}_{\langle p_1,p_2,p_3,p_4\rangle}}, \acute{E})$ and $(\tilde{\mathfrak{F}}_{\dot{s}^{\wedge}_{\langle p_1,p_2,p_3,p_4\rangle}}, \acute{E}) \tilde{\cap} (\tilde{L}_{\dot{s}^{\wedge}_{\langle p_1,p_2,p_3,p_4\rangle}}, \acute{E}) \cong \tilde{\Phi}$. Clearly, $\{\left(\tilde{\mathfrak{F}}_{\dot{s}^{\wedge}_{\langle p_1,p_2,p_3,p_4\rangle}}, \acute{E}\right) : \dot{s}^{\wedge}_{\langle p_1,p_2,p_3,p_4\rangle} \in (\tilde{\mathfrak{L}}, \acute{E})\}$ is QPNS p-OC of $(\tilde{\mathfrak{L}}, \acute{E})$ and $(\tilde{\mathfrak{L}}, \acute{E})$ being soft QPNS p-compact there exists finitely many points $\dot{s}_1{}^{\wedge}_{\langle p_1,p_2,p_3,p_4\rangle}, \dot{s}_2{}^{\wedge}_{\langle p_1,p_2,p_3,p_4\rangle}, \dot{s}_3{}^{\wedge}_{\langle p_1,p_2,p_3,p_4\rangle}, \dot{s}_4{}^{\wedge}_{\langle p_1,p_2,p_3,p_4\rangle}, \ldots\ldots\ldots \dot{s}_n{}^{\wedge}_{\langle p_1,p_2,p_3,p_4\rangle}$in $(\tilde{\mathfrak{L}}, \acute{E})$ such that $(\tilde{\mathfrak{L}}, \acute{E}) \tilde{\subseteq} \cup_{i=1}^{n} \left(\tilde{\mathfrak{F}}_{\dot{s}_i{}^{\wedge}_{\langle p_1,p_2,p_3,p_4\rangle}}, \acute{E}\right)$. Let $(\tilde{\mathfrak{F}}, \acute{E}) \cong \cup_{i=1}^{n} \left(\tilde{\mathfrak{F}}_{\dot{s}_i{}^{\wedge}_{\langle p_1,p_2,p_3,p_4\rangle}}, \acute{E}\right)$ and $(\tilde{L}, \acute{E}) \cong \cap_{i=1}^{n} \left(\tilde{L}_{\dot{s}_i{}^{\wedge}_{\langle p_1,p_2,p_3,p_4\rangle}}, \acute{E}\right)$. Then, $(\tilde{\mathfrak{L}}, \acute{E}) \tilde{\subseteq} (\tilde{\mathfrak{F}}, \acute{E})$ and $(\tilde{\varpi}, \acute{E}) \tilde{\subseteq} (\tilde{L}, \acute{E})$. Since $(\tilde{\mathfrak{F}}, \acute{E}) \tilde{\subseteq} \left(\tilde{L}_{\dot{s}_i{}^{\wedge}_{\langle p_1,p_2,p_3,p_4\rangle}}, \acute{E}\right)$ for each i. Clearly, $(\tilde{\mathfrak{F}}, \acute{E})$ and $(\tilde{L}, \acute{E})$ are QPNS p-open sets. Also, $(\tilde{\mathfrak{F}}, \acute{E}) \tilde{\cap} (\tilde{L}, \acute{E}) \tilde{\cong}, (\tilde{\mathfrak{F}}, \acute{E}) \tilde{\cap} (\tilde{L}, \acute{E}) \cong \tilde{\Phi}$,for, if $y^{\wedge}_{\langle p_1,p_2,p_3,p_4\rangle} \in (\tilde{\mathfrak{F}}, \acute{E})$ implies $y^{\wedge}_{\langle p_1,p_2,p_3,p_4\rangle} \in \left(\tilde{\mathfrak{F}}_{\dot{s}_i{}^{\wedge}_{\langle p_1,p_2,p_3,p_4\rangle}}, \acute{E}\right)$ for some $\dot{s}^{\wedge}_{\langle p_1,p_2,p_3,p_4\rangle_i}$ implies $y^{\wedge}_{\langle p_1,p_2,p_3,p_4\rangle} \notin \left(\tilde{L}_{\dot{s}_i{}^{\wedge}_{\langle p_1,p_2,p_3,p_4\rangle}}, \acute{E}\right)$ implies $y^{\wedge}_{\langle p_1,p_2,p_3,p_4\rangle} \notin \cap_{i=1}^{n} \left(\tilde{L}_{\dot{s}_i{}^{\wedge}_{\langle p_1,p_2,p_3,p_4\rangle}}, \acute{E}\right)$ implies $y^{\wedge}_{\langle p_1,p_2,p_3,p_4\rangle} \notin (\tilde{L}, \acute{E})$.

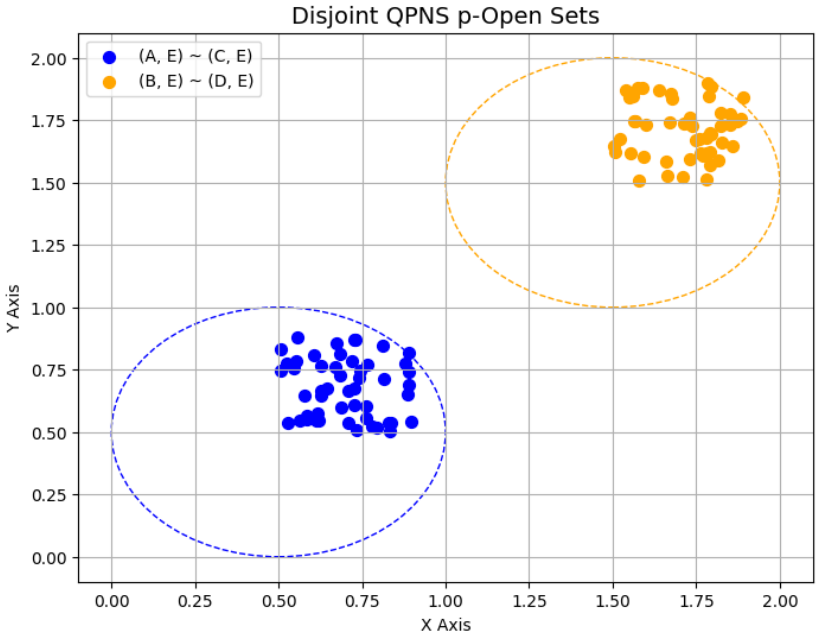

Fig: 4.7

Theorem 4.10 Let $(\tilde{Y}, \tau_1, \tau_2, \acute{E})$ be a QPNS sub-space of $(\tilde{U}, \tau_3, \tau_4, \acute{E})$ then $\tilde{Y}$ is QPNS p-cover w.r.t the QPNSBTS $\tau_1 U \tau_2$ iff $\tilde{Y}$ is QPNS p- covers w.r.t. the QPNSBTS $\tau_3 U \tau_4$.

Proof. Let $\left\{(\tilde{L}, \acute{E})_i : i \in I\right\}$ be a soft $\tau_1 U \tau_2$QPNS p-open cover of$\tilde{Y}$, then $\tilde{Y} \tilde{\subseteq} \coprod_{i\in I}(\tilde{L}, \acute{E})_i$ this implies$(\tilde{L}, \acute{E})_i \in \tau_1 U \tau_2$ implies there exists$(\tilde{\sigma}, \acute{E})_i \in \tau_3 U \tau_4$ such that $(\tilde{L}, \acute{E})_i = (\tilde{\sigma}, \acute{E})_i \cap (\tau_3 U \tau_4)$ such that $(\tilde{L}, \acute{E})_i = (\tilde{\sigma}, \acute{E})_i \cap \tilde{Y} \tilde{\subseteq} (\tilde{\sigma}, \acute{E})_i$ implies there exists $(\tilde{\sigma}, \acute{E})_i \in \tau_3 U \tau_4$ such that $(\tilde{L}, \acute{E})_i \tilde{\subseteq} (\tilde{\sigma}, \acute{E})_i$ implies $\coprod_{i\in I}(\tilde{L}, \acute{E})_i \tilde{\subseteq} \coprod_{i\in I}(\tilde{\sigma}, \acute{E})_i$. But $\tilde{Y} \tilde{\subseteq} \coprod_{i\in I}(\tilde{L}, \acute{E})_i$ so that $\tilde{Y} \tilde{\subseteq} \coprod_{i\in I}(\tilde{\sigma}, \acute{E})_i$ .This proves $\coprod_{i\in I}(\tilde{\sigma}, \acute{E})_i$ is soft $(\tau_3 U \tau_4)$QPNS p-open cover of $\tilde{Y}$ which is known to be QPNS p-compact w.r.t. $(\tau_3 U \tau_4)$ and hence the QPNS cover $\left\{(\tilde{\sigma}, \acute{E})_i : i \in I\right\}$ must be shrinkable to a finite QPNS sub-cover, say, $\left\{(\tilde{\sigma}, \acute{E})_{ir} : r = 1,2,3, \dots, n\right\}$ then $\tilde{Y} \tilde{\subseteq} \coprod_{r\tilde{\cong}\tilde{1}}^{\tilde{n}}(\tilde{\sigma}, \acute{E})_{i_r}$from which $\tilde{Y} \cap \tilde{Y} \tilde{\subseteq} \tilde{Y} \cap \left(\coprod_{r\tilde{\cong}\tilde{1}}^{\tilde{n}}(\tilde{\sigma}, \acute{E})_{i_r}\right) = \coprod_{r\tilde{\cong}\tilde{1}}^{\tilde{n}}(\tilde{Y} \cap (\tilde{\sigma}, \acute{E})_{i_r}) = \left(\coprod_{r\tilde{\cong}\tilde{1}}^{\tilde{n}}(\tilde{L}, \acute{E})_{i_r}\right)$ or $\tilde{Y} \tilde{\subseteq} \coprod_{r\tilde{\cong}\tilde{1}}^{\tilde{n}}(\tilde{L}, \acute{E})_{i_r}$ this shows that $\left\{(\tilde{L}, \acute{E})_{ir} : 1 \leq r \leq n\right\}$ is soft $(\tau_1 U \tau_2)$ open-cover of $\tilde{Y}$.Hence $\tilde{Y}$is QPNS p-compact. Conversely, Let $(\tilde{\tilde{Y}}, \tau_1, \tau_2, \acute{E})$ is QPNSsub-space of $(\tilde{U}, \tau_3, \tau_4, \acute{E})$. Also suppose that $\tilde{Y}$is QPNS p-compact. To prove that $\tilde{Y}$is QPNS p-compact. Let $\left\{(\tilde{\sigma}, \acute{E})_i : i \in I\right\}$ be soft $\tau_3 U \tau_4$ open cover of $\tilde{Y}$so that $\tilde{Y} \tilde{\subseteq} \coprod_{i\in I}(\tilde{\sigma}, \acute{E})_i$ from which $\tilde{Y} \cap \tilde{Y} \tilde{\subseteq} \tilde{Y} \cap \left(\coprod_{r\tilde{\cong}\tilde{1}}^{\tilde{n}}(\tilde{\sigma}, \acute{E})_i\right)$ or $\tilde{Y} \cap \left(\coprod_{r\tilde{\cong}\tilde{1}}^{\tilde{n}}(\tilde{Y} \cap (\tilde{\sigma}, \acute{E})_i\right)$ on taking $(\tilde{L}, \acute{E})_i = (\tilde{Y} \cap (\tilde{\sigma}, \acute{E})_i$ we get$\tilde{Y} \tilde{\subseteq} \left(\coprod_{r\tilde{\cong}\tilde{1}}^{\tilde{n}}(\tilde{L}, \acute{E})_i\right)$. $(\tilde{\sigma}, \acute{E})_i \in \tau_3 U \tau_4$implies that $(\tilde{L}, \acute{E})_i = \tilde{Y} \cap \left(\coprod_{r\tilde{\cong}\tilde{1}}^{\tilde{n}}(\tilde{\sigma}, \acute{E})_i\right) \in (\tau_3 U \tau_4)$ so it is clear that $\left\{(\tilde{L}, \acute{E})_i : i \in I\right\}$ is $(\tau_3 U \tau_4)$QPNS p-open cover $\tilde{\tilde{Y}}$ which is known to be $(\tau_3 U \tau_4)$QPNS p-compact and hence this soft cover must be reducible to QPNS finite sub-cover say $\left\{(\tilde{L}, \acute{E})_{ir} : 1 \leq r \leq n\right\}$. this implies $\tilde{Y} \tilde{\subseteq} \left(\coprod_{r\tilde{\cong}\tilde{1}}^{\tilde{n}}(\tilde{L}, \acute{E})_i\right) = \left(\coprod_{r\tilde{\cong}\tilde{1}}^{\tilde{n}}(\tilde{\subseteq} \cap (\tilde{\sigma}, \acute{E})_{ir}\right)$ or $\tilde{Y} \tilde{\subseteq} \left(\coprod_{r\tilde{\cong}\tilde{1}}^{\tilde{n}}(\tilde{Y} \cap (\tilde{\sigma}, \acute{E})_{ir}\right) \tilde{\subseteq} \left(\coprod_{r\tilde{\cong}\tilde{1}}^{\tilde{n}}(\tilde{\sigma}, \acute{E})_{i_r}\right)$ or $\tilde{Y} \tilde{\subseteq} \left(\coprod_{r\tilde{\cong}\tilde{1}}^{\tilde{n}}(\tilde{\sigma}, \acute{E})_{i_r}\right)$ this shows $(\tau_3 U \tau_4)$QPNS p-compact.

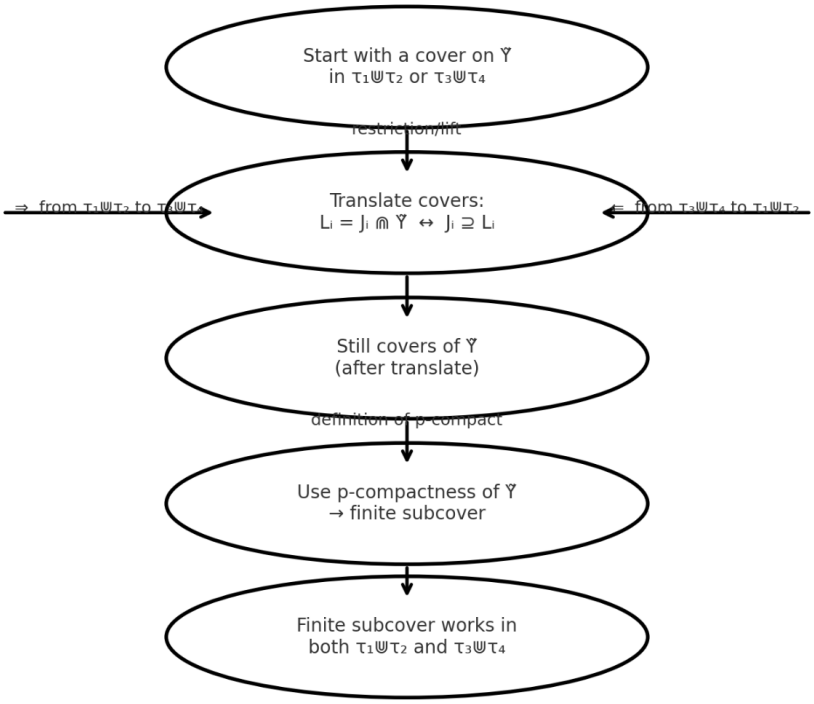
Start with a cover on Ϋ
in τ₁⋓τ₂ or τ₃⋓τ₄
restriction/lift
⇒ from τ₁⋓τ₂ to τ₃⋓τ₄
Translate covers:
Lᵢ = Jᵢ ⋒ Ϋ ↔ Jᵢ ⊇ Lᵢ
⇐ from τ₃⋓τ₄ to τ₁⋓τ₂
Still covers of Ϋ
(after translate)
definition of p-compact
Use p-compactness of Ϋ
→ finite subcover
Finite subcover works in
both τ₁⋓τ₂ and τ₃⋓τ₄

Fig: 4.8

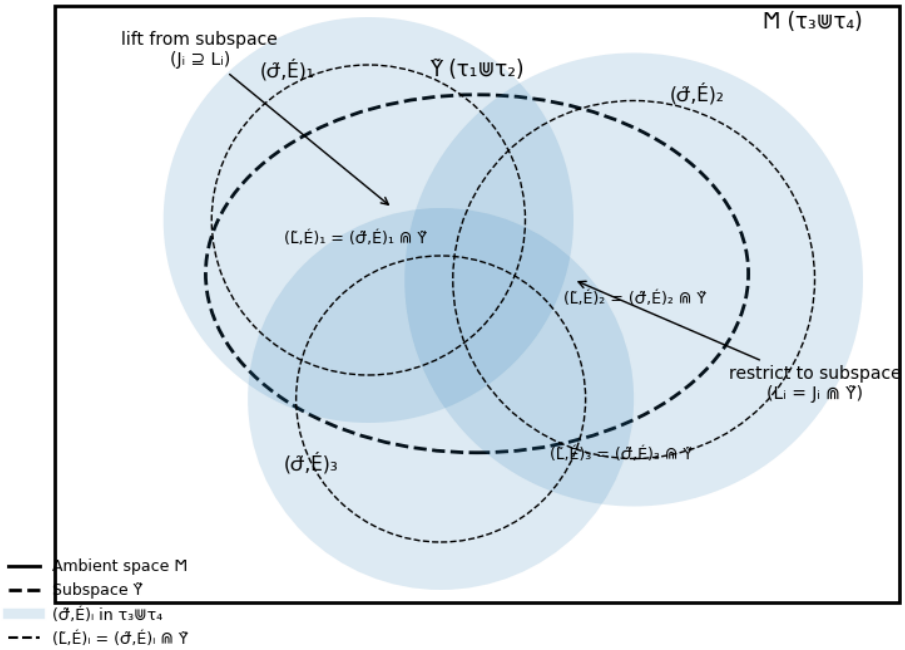
M (τ₃⋓τ₄)
lift from subspace
(Jᵢ ⊇ Lᵢ)
(ð,É)₁
Ϋ (τ₁⋓τ₂)
(ð,É)₂
(Ł,É)₁ = (ð,É)₁ ⋒ Ϋ
(Ł,É)₂ = (ð,É)₂ ⋒ Ϋ
restrict to subspace
(Lᵢ = Jᵢ ⋒ Ϋ)
(ð,É)₃
(Ł,É)₃ = (ð,É)₃ ⋒ Ϋ
Ambient space M
Subspace Ϋ
(ð,É)ᵢ in τ₃⋓τ₄
(Ł,É)ᵢ = (ð,É)ᵢ ⋒ Ϋ

Fig: 4.9

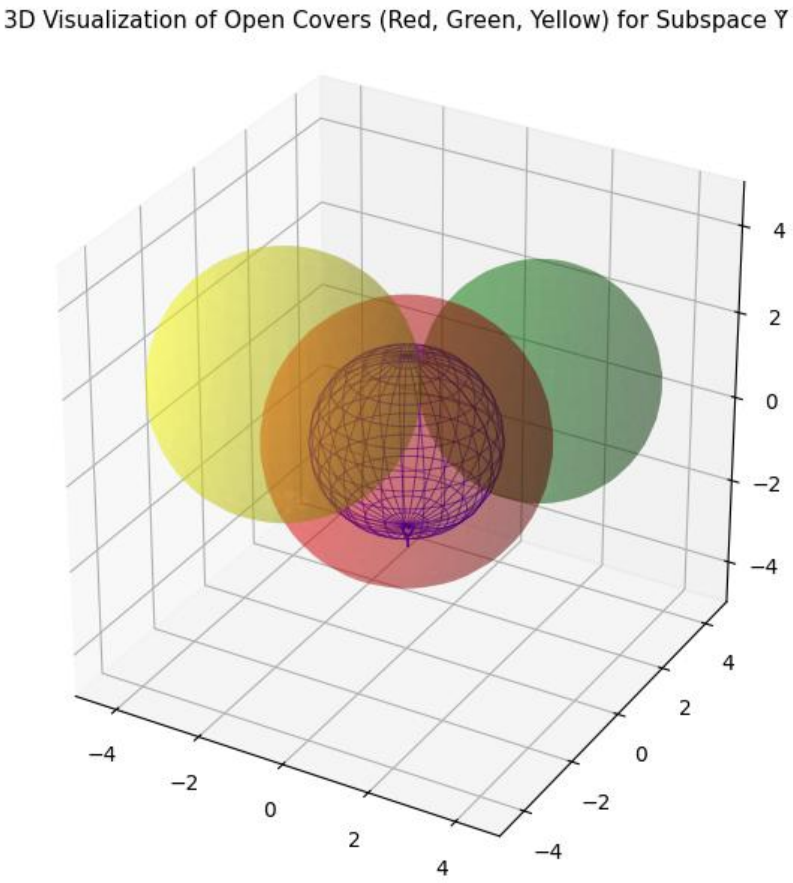

Fig: 4.10

5. Exploring tangent similarity measure for enhanced data classification and pattern recognition

One analytical technique for determining the degree of similarity between two vectors (data) is the tangent similarity measure (TSM). It is widely used in a variety of machine learning, image processing, and data analysis applications. By taking into account the geometric orientation of the data points, TSM will be able to uncover hidden patterns and associations that would have been impossible to find with just distance-based measurements. It is frequently used in data analysis, machine learning, and image processing. In the context of a military mission, TSM can be used to classified potential targets based on surveillance data. This is accomplished by contrasting a target's operational characteristics with the currently available categorized profiles. The likelihood of comparing and classifying threats is then increased, and the degree to which a target is classified into pre-established threat classifications is estimated. The classification and pattern recognition tasks are aided by a number of machine learning and visualization measures. Sig: K-means++ algorithm, Restricted Boltzmann Machine (RBM),GLO,

LDA, ICA, K-Means clustering to the IRIS, Bar graph,3D-Bar Graph, PC for a 3D t-SNE transformation, CC, FDA, FPC.

5.1 Tan similarity measures:

Let $Ⱨ_i = (AbT_{ik}, ReT_{ik}, ReF_{ik}, AbF_{ik})$, $Ⱨ_j = \left(AbT_{jk}, ReT_{jk}, ReF_{jk}, AbF_{jk}\right)$ are two DNSSs. Each set is represented by four components for each feature k:

AbT_{ik}: Absolute truth membership of feature k for $Ⱨ_i$.

ReT_{ik}: Relative truth membership degree of feature k for $Ⱨ_i$.

ReF_{ik}: Relative false membership degree of feature k for $Ⱨ_i$.

AbF_{ik}: Absolute false membership degree of feature k for $Ⱨ_i$.

The values typically satisfy: $AbT_{ik}, ReT_{ik}, ReF_{ik}, AbF_{ik} \in [0,1]$

Similarly, for object $Ⱨ_j$:

AbT_{ik}: Absolute truth membership of feature k for $Ⱨ_j$.

ReT_{ik}: Relative truth membership degree of feature k for $Ⱨ_j$.

ReF_{ik}: Relative false membership degree of feature k for $Ⱨ_j$.

AbF_{ik}: Absolute false membership degree of feature k for $Ⱨ_j$.

The values typically satisfy: $AbT_{jk}, ReT_{jk}, ReF_{jk}, AbF_{jk} \in [0,1]$

The tangent similarity measure between $Ⱨ_i$ and $Ⱨ_j$ is defined as:

$$Tangent_{QNSS}(Ⱨ_i, Ⱨ_j) =$$

$$\frac{1}{n}\sum_{i=1}^{n}\left\{1 - tan\frac{\pi}{12}\left(\left|AbT_{ik} - AbT_{jk}\right| + \left|ReT_{ik} - ReT_{jk}\right| + \left|ReF_{ik} - ReF_{jk}\right| + \left|AbF_{ik} - AbF_{jk}\right|\right)\right\}.$$

5.2 Tangent similarity in military target classification and machine learning

One analytical technique for determining how similar two vectors (data) are to one another is the tangent similarity measure (TSM). It has numerous uses in data analysis, image processing, and machine learning. TSM can provide information on latent patterns and associations that are not visible when utilizing distance-based measurements because of the geometric orientation of the data points. In military applications, TSM can also be used to classify potential targets based on surveillance data.

Comparing an object of interest's operating characteristics to pre-existing profiles is how this is done. Both the likelihood of accurately comparing and classifying the risks and the degree to which a target is categorized within pre-existing danger categories are raised. Tasks involving pattern recognition and classification can benefit from a variety of machine learning and visualization approaches.

Principal Component Analysis (PCA) of the IRIS data reduces the dimensionality of the data by transforming features into orthogonal components; Neutrosophic PCA can model the uncertainty in variance contribution or feature relationship that may be indeterminate; t-Distributed Stochastic Neighbor Embedding (t-SNE) is used to visualize the data in 2D or 3D,

and the data may have a high number of dimensions; a neutrosophic t-SNE would deal with an ambiguous cluster boundary by using truth, indeterminacy, and falsity memberships in similarity calculations; K-Means++ Clustering improves the initial centroid choice; and neutrosophic K-Means++ can place data points into the clusters in varying membership degrees, indeterminacy, and non-membership, which improves cluster validity.

Generative neural networks that learn features are called Restricted Boltzmann Machines (RBMs). A neutrosophic RBM can model neutrosophic arbitrary activations as a kind of hidden layers. Neutrosophic restrictions may be used to solve the goals with unknown parameters in Global Linear Optimization (GLO), which tackles problems globally. Although it can be used to model feature space subjects, Latent Dirichlet Allocation (LDA) is most frequently used to text. There may be ambiguous subject allocations for neutrophilic LDA. Mixed signals are separated into individual components via ICA. Neutrosophic ICA can resolve component independence or mixing matrix ambiguity.

K-Means normalization of IRIS data Features are scaled by clustering. Uncertainty in scaled values or grouping assignments may also be handled via the neutrosophic K-Means. Although neutrosophic versions may convey truth, indeterminacy, and falsity memberships between classes or features, Bar Graphs and 3D Bar Graphs are used to represent distributions. In 3D t-SNE, the multivariate data is displayed using parallel coordinates. These could be neutrosophic t-SNE ambiguous pathways through dimensions. Original data points and smooth spline functions are used to illustrate trends. Neutrosophic splines can be represented by curves with uncertain smoothing parameters or uncertain fits. Neutrosophic FPCA may produce Eigen-functions utilizing uncertain functional data, and the IRIS data has Functional Principal Components (Eigen-functions) to functional data.

5.3 Visualizing complexity: PCA, t-SNE, UMAP, and ICA applications

Assume that we have knowledge of a set of potential military targets, specifically $T = \{T_1, T_2, T_3, T_4\}$, which is a particular operationally significant object. It could be a convoy of supplies, a collection of man-made parts, a mobile command center, or even a communications hub. A collection of surveillance or reconnaissance data $S = \{S_1, S_2, S_3, S_4\}$ can be assigned to each target. Radar signatures, thermal imaging, electronic emission monitoring, and movement observation are a few examples of sufficient sources of this type of information.

These crucial intelligence leads aid in the identification and description of every target. Every target has been touched or indexed: $C = \{C_1, C_2, C_3, C_4\}$.. These categories could include communication hubs, logistical clusters, mobile decoys, and high-value strategic assets that must be removed or dealt with right away. Each target's working attribute consists of the following four structural components: The deviations of the grating's appealing pattern on an electrical or thermal surface are measured by AbS (Abnormal Signal Signature).

The target signal's proximity to anticipated threat parameters is measured by RelT (Relevant Threat Threshold). Abnormal Fluctuation (AbF) is the abnormal change in the target behavior or sign, whereas RelF (Relative Fluctuation) is the change of the electronic or thermal signal employed in operating dynamic. Each target will be modeled as a feature vector based on these criteria. The cotangent similarity metric is then used to compare this to the other vectors of known targets. When two vectors are involved, the cosine of the angle represents the similarity score. The likelihood that the current target falls into a known threat profile increases with the cosine value's proximity to 1. The targets can be automatically classified into the high accuracy category in real-time by comparing the surveillance data with the threat models that are currently in use. As a result, the decision-makers may quickly identify their targets, assess their danger level, and rank them according to how crucial they are for engagement or surveillance. To improve combat field intelligence and guarantee quicker, evidence-based decision-making, the software is used in fluid generation workplaces.

Table 5.3.1: Tangent similarity matrix for target intelligence feature extraction (T × S)

	S_1	S_2	…	S_n
T_1	$AbT_{11}, RelT_{11},$ $RelF_{11}, AbF_{11}$	$AbT_{12}, RelT_{12},$ $RelF_{12}, AbF_{12}$	…	$AbT_{1n}, RelT_{1n},$ $RelF_{1n}, AbF_{1n}$
T_2	$AbT_{21}, RelT_{21},$ $RelF_{21}, AbF_{21}$	$AbT_{22}, RelT_{22}$ $RelF_{21}, AbF_{22}$	…	$AbT_{2n}, RelT_{2n},$ $RelF_{2n}, AbF_{2n}$
…	…	…	…	…
T_m	$AbT_{m1}, RelT_{m1},$ $RelF_{m1}, AbF_{m1}$	$AbT_{m2}, RelT_{m2},$ $RelF_{m2}, AbF_{m2}$	…	$AbT_{mn}, RelT_{mn},$ $RelF_{mn}, AbF_{mn}$

The un-coded surveillance parameters of every target T_i gathered by every data source S_i are displayed in this table. AbS (Abnormal Signature), RelT (Relevant Threat Threshold), RelF (Relative Fluctuation), and AbF (Abnormal Fluctuation) are used to simulate a threat for each target-source combination by providing a thorough examination of the 4-dimensional feature vectors at each cell.

Table 5.3.2: Analytical matrix for operational target detection and classification (T × S → C)

Row-I	S_1	S_2	S_3	S_4	**Row-II**	C_1	C_2	C_3	C_4
T_1	$\begin{pmatrix}0.5\\0.7\\0.3\\0.4\end{pmatrix}$	$\begin{pmatrix}0.6\\0.4\\0.3\\0.8\end{pmatrix}$	$\begin{pmatrix}0.3\\0.5\\0.8\\0.9\end{pmatrix}$	$\begin{pmatrix}0.9\\0.2\\0.4\\0.6\end{pmatrix}$	S_1	$\begin{pmatrix}0.3\\0.5\\0.7\\0.8\end{pmatrix}$	$\begin{pmatrix}0.7\\0.6\\0.2\\0.3\end{pmatrix}$	$\begin{pmatrix}0.5\\0.4\\0.6\\0.9\end{pmatrix}$	$\begin{pmatrix}0.3\\0.2\\0.4\\0.7\end{pmatrix}$
T_2	$\begin{pmatrix}0.4\\0.7\\0.5\\0.7\end{pmatrix}$	$\begin{pmatrix}0.2\\0.4\\0.6\\0.9\end{pmatrix}$	$\begin{pmatrix}0.3\\0.4\\0.5\\0.8\end{pmatrix}$	$\begin{pmatrix}0.7\\0.4\\0.6\\0.4\end{pmatrix}$	S_2	$\begin{pmatrix}0.2\\0.3\\0.7\\0.8\end{pmatrix}$	$\begin{pmatrix}0.6\\0.7\\0.4\\0.5\end{pmatrix}$	$\begin{pmatrix}0.3\\0.6\\0.8\\0.4\end{pmatrix}$	$\begin{pmatrix}0.4\\0.3\\0.6\\0.2\end{pmatrix}$
T_3	$\begin{pmatrix}0.7\\0.6\\0.8\\0.3\end{pmatrix}$	$\begin{pmatrix}0.2\\0.8\\0.7\\0.5\end{pmatrix}$	$\begin{pmatrix}0.6\\0.3\\0.2\\0.4\end{pmatrix}$	$\begin{pmatrix}0.6\\0.2\\0.7\\0.3\end{pmatrix}$	S_3	$\begin{pmatrix}0.4\\0.7\\0.5\\0.6\end{pmatrix}$	$\begin{pmatrix}0.6\\0.3\\0.4\\0.5\end{pmatrix}$	$\begin{pmatrix}0.7\\0.3\\0.2\\0.4\end{pmatrix}$	$\begin{pmatrix}0.5\\0.6\\0.3\\0.4\end{pmatrix}$
T_4	$\begin{pmatrix}0.4\\0.6\\0.8\\0.3\end{pmatrix}$	$\begin{pmatrix}0.3\\0.6\\0.2\\0.9\end{pmatrix}$	$\begin{pmatrix}0.5\\0.8\\0.4\\0.3\end{pmatrix}$	$\begin{pmatrix}0.4\\0.6\\0.8\\0.4\end{pmatrix}$	S_4	$\begin{pmatrix}0.3\\0.6\\0.4\\0.8\end{pmatrix}$	$\begin{pmatrix}0.9\\0.3\\0.2\\0.5\end{pmatrix}$	$\begin{pmatrix}0.4\\0.3\\0.8\\0.6\end{pmatrix}$	$\begin{pmatrix}0.3\\0.8\\0.9\\0.4\end{pmatrix}$

This table displays the cotangent similarity values based on the target feature vectors and a comparison with the targets' known operational characteristics (e.g., C_1: high-value asset, C_2: decoy, C_3: communication node, C_4: logistical unit). The un-normalized cosine similarity between each target (T) and its surveillance data (S) is provided in Row-I (T × S). In the meantime, the cotangent proximity of each data source foreground to the classified operation profile is displayed in Row-II (S × C). By classifying or grouping the targets into groups based on the sort of threat they are associated to or the type of operations they are involved in, the provided approach enables prioritizing the actions (attack, monitor, ignore, etc.). $Ⱨ_i$ and $Ⱨ_j$have the following tangent similarity:

$$Tangent_{QNSS}(Ⱨ_i, Ⱨ_j) =$$

$$\frac{1}{n}\sum_{i=1}^{n}\left\{1 - tan\frac{\pi}{12}\left(\left|AbT_{ik} - AbT_{jk}\right| + \left|ReT_{ik} - ReT_{jk}\right| + \left|ReF_{ik} - ReF_{jk}\right| + \left|AbF_{ik} - AbF_{jk}\right|\right)\right\}.$$

For $n = 4$ then $R_1 + C_1 \Rightarrow Tan_{QPNSS}(Ⱨ_i, Ⱨ_j) =$

$$\begin{aligned}
&\frac{1}{4}\left\{1 - \tan\frac{\pi}{12}(|0.5 - 0.3| + |0.7 - 0.5| + |0.3 - 0.7| + |0.4 - 0.8|)\right\}\\
&+\frac{1}{4}\left\{1 - \tan\frac{\pi}{12}(|0.6 - 0.2| + |0.4 - 0.3| + |0.3 - 0.7| + |0.8 - 0.8|)\right\}\\
&+\frac{1}{4}\left\{1 - \tan\frac{\pi}{12}(|0.3 - 0.4| + |0.5 - 0.7| + |0.8 - 0.5| + |0.9 - 0.6|)\right\}\\
&+\frac{1}{4}\left\{1 - \tan\frac{\pi}{12}(|0.9 - 0.3| + |0.2 - 0.6| + |0.4 - 0.4| + |0.6 - 0.8|)\right\}\\
&= 0.1687 + 0.1900 + 0.1900 + 0.1687 = 0.7174
\end{aligned}$$

For $n = 4$ then $R_1 + C_2 \Rightarrow Tan_{QPNSS}(\text{Ⱨ}_i, \text{Ⱨ}_j) =$

$$\frac{1}{4}\left\{1 - \tan\frac{\pi}{12}(|0.5-0.7| + |0.7-0.6| + |0.3-0.2| + |0.4-0.3|)\right\}$$
$$+\frac{1}{4}\left\{1 - \tan\frac{\pi}{12}(|0.6-0.6| + |0.4-0.7| + |0.3-0.4| + |0.8-0.5|)\right\}$$
$$+\frac{1}{4}\left\{1 - \tan\frac{\pi}{12}(|0.3-0.6| + |0.5-0.3| + |0.8-0.4| + |0.9-0.5|)\right\}$$
$$+\frac{1}{4}\left\{1 - \tan\frac{\pi}{12}(|0.9-0.9| + |0.2-0.3| + |0.4-0.2| + |0.6-0.5|)\right\}$$
$$= 0.2171 + 0.2036 + 0.1614 + 0.2237 = 0.8058$$

For $n = 4$ then $R_1 + C_3 \Rightarrow Tan_{QPNSS}(\text{Ⱨ}_i, \text{Ⱨ}_j) =$

$$\frac{1}{4}\left\{1 - \tan\frac{\pi}{12}(|0.5-0.5| + |0.7-0.4| + |0.3-0.6| + |0.4-0.9|)\right\}$$
$$+\frac{1}{4}\left\{1 - \tan\frac{\pi}{12}(|0.6-0.3| + |0.4-0.6| + |0.3-0.8| + |0.8-0.4|)\right\}$$
$$+\frac{1}{4}\left\{1 - \tan\frac{\pi}{12}(|0.3-0.7| + |0.5-0.3| + |0.8-0.2| + |0.9-0.4|)\right\}$$
$$+\frac{1}{4}\left\{1 - \tan\frac{\pi}{12}(|0.9-0.4| + |0.2-0.3| + |0.4-0.8| + |0.6-0.6|)\right\}$$
$$= 0.1759 + 0.1540 + 0.1307 + 0.1830 = 0.6436$$

For $n = 4$ then $R_1 + C_4 \Rightarrow Tan_{QPNSS}(\text{Ⱨ}_i, \text{Ⱨ}_j) =$

$$\frac{1}{4}\left\{1 - \tan\frac{\pi}{12}(|0.5-0.3| + |0.7-0.2| + |0.3-0.4| + |0.4-0.7|)\right\}$$
$$+\frac{1}{4}\left\{1 - \tan\frac{\pi}{12}(|0.6-0.4| + |0.4-0.3| + |0.3-0.6| + |0.8-0.2|)\right\}$$
$$+\frac{1}{4}\left\{1 - \tan\frac{\pi}{12}(|0.3-0.5| + |0.5-0.6| + |0.8-0.3| + |0.9-0.4|)\right\}$$
$$+\frac{1}{4}\left\{1 - \tan\frac{\pi}{12}(|0.9-0.3| + |0.2-0.8| + |0.4-0.9| + |0.6-0.4|)\right\}$$
$$= 0.1759 + 0.1687 + 0.1614 + 0.1142 = 0.6202$$

For $n = 4$ then $R_2 + C_1 \Rightarrow Tan_{QPNSS}(\text{Ⱨ}_i, \text{Ⱨ}_j) =$

$$\frac{1}{4}\left\{1 - \tan\frac{\pi}{12}(|0.4-0.3| + |0.7-0.5| + |0.5-0.7| + |0.7-0.8|)\right\}$$
$$+\frac{1}{4}\left\{1 - \tan\frac{\pi}{12}(|0.2-0.2| + |0.4-0.3| + |0.6-0.7| + |0.9-0.8|)\right\}$$
$$+\frac{1}{4}\left\{1 - \tan\frac{\pi}{12}(|0.3-0.4| + |0.4-0.7| + |0.5-0.5| + |0.8-0.6|)\right\}$$
$$+\frac{1}{4}\left\{1 - \tan\frac{\pi}{12}(|0.7-0.3| + |0.4-0.6| + |0.6-0.4| + |0.4-0.8|)\right\}$$
$$= 0.2104 + 0.2303 + 0.2104 + 0.1687 = 0.8198$$

For $n = 4$ then $R_2 + C_2 \Rightarrow Tan_{QPNSS}(\text{Ⱨ}_i, \text{Ⱨ}_j) =$

$$\frac{1}{4}\left\{1-\tan\frac{\pi}{12}(|0.4-0.7|+|0.7-0.6|+|0.5-0.2|+|0.7-0.3|)\right\}$$
$$+\frac{1}{4}\left\{1-\tan\frac{\pi}{12}(|0.2-0.6|+|0.4-0.7|+|0.6-0.4|+|0.9-0.5|)\right\}$$
$$+\frac{1}{4}\left\{1-\tan\frac{\pi}{12}(|0.3-0.6|+|0.4-0.3|+|0.5-0.4|+|0.8-0.5|)\right\}$$
$$+\frac{1}{4}\left\{1-\tan\frac{\pi}{12}(|0.7-0.9|+|0.4-0.3|+|0.6-0.2|+|0.4-0.5|)\right\}$$
$$=0.1759+0.1614+0.1968+0.1968=0.7309$$

For $n=4$ then $R_2+C_3 \Rightarrow Tan_{QPNSS}(\text{Ⱨ}_i,\text{Ⱨ}_j)=$

$$\frac{1}{4}\left\{1-\tan\frac{\pi}{12}(|0.4-0.5|+|0.7-0.4|+|0.5-0.6|+|0.7-0.9|)\right\}$$
$$+\frac{1}{4}\left\{1-\tan\frac{\pi}{12}(|0.2-0.3|+|0.4-0.6|+|0.6-0.8|+|0.9-0.4|)\right\}$$
$$+\frac{1}{4}\left\{1-\tan\frac{\pi}{12}(|0.3-0.7|+|0.4-0.3|+|0.5-0.2|+|0.8-0.4|)\right\}$$
$$+\frac{1}{4}\left\{1-\tan\frac{\pi}{12}(|0.7-0.4|+|0.4-0.3|+|0.6-0.8|+|0.4-0.6|)\right\}$$
$$=0.2036+0.1830+0.1687+0.1968=0.7521$$

For $n=4$ then $R_2+C_4 \Rightarrow Tan_{QPNSS}(\text{Ⱨ}_i,\text{Ⱨ}_j)=$

$$\frac{1}{4}\left\{1-\tan\frac{\pi}{12}(|0.4-0.3|+|0.7-0.2|+|0.5-0.4|+|0.7-0.7|)\right\}$$
$$+\frac{1}{4}\left\{1-\tan\frac{\pi}{12}(|0.2-0.4|+|0.4-0.3|+|0.6-0.6|+|0.9-0.2|)\right\}$$
$$+\frac{1}{4}\left\{1-\tan\frac{\pi}{12}(|0.3-0.5|+|0.4-0.6|+|0.5-0.3|+|0.8-0.4|)\right\}$$
$$+\frac{1}{4}\left\{1-\tan\frac{\pi}{12}(|0.7-0.3|+|0.4-0.8|+|0.6-0.9|+|0.4-0.4|)\right\}$$
$$=0.2036+0.1830+0.1830+0.1759=0.7455$$

For $n=4$ then $R_3+C_1 \Rightarrow Tan_{QPNSS}(\text{Ⱨ}_i,\text{Ⱨ}_j)=$

$$\frac{1}{4}\left\{1-\tan\frac{\pi}{12}(|0.7-0.3|+|0.6-0.5|+|0.8-0.7|+|0.3-0.8|)\right\}$$
$$+\frac{1}{4}\left\{1-\tan\frac{\pi}{12}(|0.2-0.2|+|0.8-0.3|+|0.7-0.7|+|0.5-0.8|)\right\}$$
$$+\frac{1}{4}\left\{1-\tan\frac{\pi}{12}(|0.6-0.4|+|0.3-0.7|+|0.2-0.5|+|0.4-0.6|)\right\}$$
$$+\frac{1}{4}\left\{1-\tan\frac{\pi}{12}(|0.6-0.3|+|0.2-0.6|+|0.7-0.4|+|0.3-0.8|)\right\}$$
$$=0.1759+0.1968+0.1759+0.1464=0.6950$$

For $n=4$ then $R_3+C_2 \Rightarrow Tan_{QPNSS}(\text{Ⱨ}_i,\text{Ⱨ}_j)=$

$$\frac{1}{4}\left\{1-\tan\frac{\pi}{12}(|0.7-0.7|+|0.6-0.6|+|0.8-0.2|+|0.3-0.3|)\right\}$$
$$+\frac{1}{4}\left\{1-\tan\frac{\pi}{12}(|0.2-0.6|+|0.8-0.7|+|0.7-0.4|+|0.5-0.5|)\right\}$$
$$+\frac{1}{4}\left\{1-\tan\frac{\pi}{12}(|0.6-0.6|+|0.3-0.3|+|0.2-0.4|+|0.4-0.5|)\right\}$$
$$+\frac{1}{4}\left\{1-\tan\frac{\pi}{12}(|0.6-0.9|+|0.2-0.3|+|0.7-0.2|+|0.3-0.5|)\right\}$$
$$=0.2104+0.1968+0.2303+0.1759=0.8134$$

For $n=4$ then $R_3+C_3 \Rightarrow Tan_{QPNSS}(\text{Ħ}_i,\text{Ħ}_j)=$

$$\frac{1}{4}\left\{1-\tan\frac{\pi}{12}(|0.7-0.5|+|0.6-0.4|+|0.8-0.6|+|0.3-0.9|)\right\}$$
$$+\frac{1}{4}\left\{1-\tan\frac{\pi}{12}(|0.2-0.3|+|0.8-0.6|+|0.7-0.8|+|0.5-0.4|)\right\}$$
$$+\frac{1}{4}\left\{1-\tan\frac{\pi}{12}(|0.6-0.7|+|0.3-0.3|+|0.2-0.4|+|0.4-0.4|)\right\}$$
$$+\frac{1}{4}\left\{1-\tan\frac{\pi}{12}(|0.6-0.4|+|0.2-0.3|+|0.7-0.8|+|0.3-0.6|)\right\}$$
$$=0.1687+0.2171+0.2303+0.2036=0.8197$$

For $n=4$ then $R_3+C_4 \Rightarrow Tan_{QPNSS}(\text{Ħ}_i,\text{Ħ}_j)=$

$$\frac{1}{4}\left\{1-\tan\frac{\pi}{12}(|0.7-0.3|+|0.6-0.2|+|0.8-0.4|+|0.3-0.7|)\right\}$$
$$+\frac{1}{4}\left\{1-\tan\frac{\pi}{12}(|0.2-0.4|+|0.8-0.3|+|0.7-0.6|+|0.5-0.2|)\right\}$$
$$+\frac{1}{4}\left\{1-\tan\frac{\pi}{12}(|0.6-0.5|+|0.3-0.6|+|0.2-0.3|+|0.4-0.4|)\right\}$$
$$+\frac{1}{4}\left\{1-\tan\frac{\pi}{12}(|0.6-0.3|+|0.2-0.8|+|0.7-0.9|+|0.3-0.4|)\right\}$$
$$=0.1387+0.1759+0.2171+0.1687=0.7004$$

For $n=4$ then $R_4+C_1 \Rightarrow Tan_{QPNSS}(\text{Ħ}_i,\text{Ħ}_j)=$

$$\frac{1}{4}\left\{1-\tan\frac{\pi}{12}(|0.4-0.3|+|0.6-0.5|+|0.8-0.7|+|0.3-0.8|)\right\}$$
$$+\frac{1}{4}\left\{1-\tan\frac{\pi}{12}(|0.3-0.2|+|0.6-0.3|+|0.2-0.7|+|0.9-0.8|)\right\}$$
$$+\frac{1}{4}\left\{1-\tan\frac{\pi}{12}(|0.5-0.4|+|0.8-0.7|+|0.4-0.5|+|0.3-0.6|)\right\}$$
$$+\frac{1}{4}\left\{1-\tan\frac{\pi}{12}(|0.4-0.3|+|0.6-0.6|+|0.8-0.4|+|0.4-0.8|)\right\}$$
$$=0.1968+0.1759+0.2104+0.1900=0.7731$$

For $n=4$ then $R_4+C_2 \Rightarrow Tan_{QPNSS}(\text{Ħ}_i,\text{Ħ}_j)=$

$$\frac{1}{4}\left\{1-\tan\frac{\pi}{12}(|0.4-0.7|+|0.6-0.6|+|0.8-0.2|+|0.3-0.3|)\right\}$$
$$+\frac{1}{4}\left\{1-\tan\frac{\pi}{12}(|0.3-0.6|+|0.6-0.7|+|0.2-0.4|+|0.9-0.5|)\right\}$$
$$+\frac{1}{4}\left\{1-\tan\frac{\pi}{12}(|0.5-0.6|+|0.8-0.3|+|0.4-0.4|+|0.3-0.5|)\right\}$$
$$+\frac{1}{4}\left\{1-\tan\frac{\pi}{12}(|0.4-0.9|+|0.6-0.3|+|0.8-0.2|+|0.4-0.5|)\right\}$$
$$=0.1900+0.1830+0.1968+0.1464=0.7162$$

For $n=4$ then $R_4+C_3 \Rightarrow Tan_{QPNSS}(\text{Ꮒ}_i, \text{Ꮒ}_j)=$

$$\frac{1}{4}\left\{1-\tan\frac{\pi}{12}(|0.4-0.5|+|0.6-0.4|+|0.8-0.6|+|0.3-0.9|)\right\}$$
$$+\frac{1}{4}\left\{1-\tan\frac{\pi}{12}(|0.3-0.3|+|0.6-0.6|+|0.2-0.8|+|0.9-0.4|)\right\}$$
$$+\frac{1}{4}\left\{1-\tan\frac{\pi}{12}(|0.5-0.7|+|0.8-0.3|+|0.4-0.2|+|0.3-0.4|)\right\}$$
$$+\frac{1}{4}\left\{1-\tan\frac{\pi}{12}(|0.4-0.4|+|0.6-0.3|+|0.8-0.8|+|0.4-0.6|)\right\}$$
$$=0.1759+0.1759+0.1830+0.2171=0.7519$$

For $n=4$ then $R_4+C_4 \Rightarrow Tan_{QPNSS}(\text{Ꮒ}_i, \text{Ꮒ}_j)=$

$$\frac{1}{4}\left\{1-\tan\frac{\pi}{12}(|0.4-0.3|+|0.6-0.2|+|0.8-0.4|+|0.3-0.7|)\right\}$$
$$+\frac{1}{4}\left\{1-\tan\frac{\pi}{12}(|0.3-0.4|+|0.6-0.3|+|0.2-0.6|+|0.9-0.2|)\right\}$$
$$+\frac{1}{4}\left\{1-\tan\frac{\pi}{12}(|0.5-0.5|+|0.8-0.6|+|0.4-0.3|+|0.3-0.4|)\right\}$$
$$+\frac{1}{4}\left\{1-\tan\frac{\pi}{12}(|0.4-0.3|+|0.6-0.8|+|0.8-0.9|+|0.4-0.4|)\right\}$$
$$=0.1614+0.1464+0.2237+0.2237=0.7552.$$

Table 5.3.3: Strategic Target Classification: Differentiating High-Value, Decoy, Communication, and Logistics Entities

Target (T)	$\boldsymbol{C_1/B_1}$ (High-value asset)	$\boldsymbol{C_2/B_2}$ (Decoy)	$\boldsymbol{C_3/B_3}$ (Communication node)	$\boldsymbol{C_4/B_4}$ (Logistical unit)
$\boldsymbol{T_1/A_1}$	0.7174	**0.8058**	0.6436	0.6202
$\boldsymbol{T_2/A_2}$	**0.8198**	0.7309	0.7521	0.7455
$\boldsymbol{T_3/A_3}$	0.6950	0.8134	**0.8197**	0.7004
$\boldsymbol{T_4/A_4}$	**0.7731**	0.7162	0.7519	0.7552

When identifying and classifying operational intelligence targets of high importance, the similarity maximums of the tangents employed in Table 5.3.3 are crucial. Predefined operation categories C 1, C 2, C 3, and C 4 have the highest correlations with the target surveillance data. The closer the target is to a specific operational category, the higher the similarity rating, which makes it easier to decide on surveillance priorities. C 1 (High-value asset): The targets that are most likely to be high-priority assets are indicated by the upper limits of this category. T 2 (0.8198) is the one that should be followed or pursued first because it is the one that is closest to C 1. C 2 (Decoy): A decoy is most likely the target here, as indicated by the high similarity value. Similar goals, like T 3 (0.8134), allow it to quickly shift its priority. Communication node C_3: Given the striking resemblance between T_3 (0.8197) and C3, it is probable that T_3 is an important node in the communication process that has to be attended to right away. C_4 (Logistical unit): The values of the top logistical units, such T_4 (0.7552), show how important it is to meet these goals in supply chain or operational logistical processes and how important it is to continuously monitor them.

6. Result and discussion

A graphic representing the first phase of the K-means++ algorithm is shown in **Fig. 6.1**. The data points are dispersed over the plot, which shows two features as representations on the axes. The different clusters are described using the yellow and purple points, which most likely indicate different data clusters. The centroids selected during the initialization procedure are indicated by red X marks. By choosing initial centrals in a way that distributes them broadly, the K-means++ method lowers the possibility of subpar clustering performance. After selecting the first centroid at random, it uses the squared distance to select subsequent centroids on the remaining data points, ensuring that they are farther apart. The initialization process's goal of predetermining the clustering is served by the centroids' noticeable separation from one another. Compared to typical randomization, this helps determine more accurate and efficient grouping.

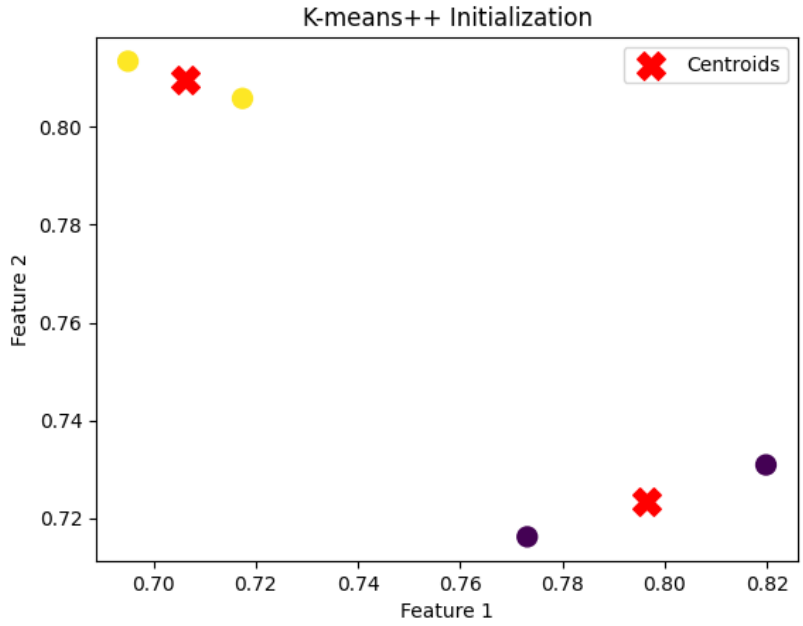

Fig 6.1

Table 6.1: For the color clarification based on the numerical values in the plot:

Color	Numerical Range (Feature 1)	Numerical Range (Feature 2)
Yellow	0.70 - 0.72	0.80 - 0.82
Purple	0.74 - 0.76	0.72 - 0.74
Red (Centroid)	0.75 - 0.78	0.75 - 0.78

This table helps to clarify the relationship between the interval of each numerical value of each attribute and the different colors used in the graphic. Higher values of Feature 2 and lower values of Feature 1 are represented by yellow points, whereas lower values of Feature 2 and higher values of Feature 1 are represented by purple points. The red centroids are positioned about in the middle of the data distribution.

A scatter plot illustrating the activations of a hidden layer's units after a Restricted Boltzmann Machine (RBM) is presented in **Fig 6.2.** The two hidden units are activated by the axes; the Hidden Unit 1 is on the x-axis, while the Hidden Unit 2 is on the y-axis. Blue dots that represent the activation values of a collection of hidden units are used to symbolize the points. The points on both the x and y axes show an increasing trend, suggesting a positive association between Hidden Units 1 and 2. The fact that both of the hidden units fall between 0.25 and 0.30 indicates that the hidden layer's units are not particularly active in this instance, which may indicate that additional training or RBM adjustment is necessary. This type of figure is commonly used in machine learning to comprehend the activation and behavior of the hidden layers of models

like RBMs, which are used for unsupervised learning processes like feature learning or dimensionality reduction.

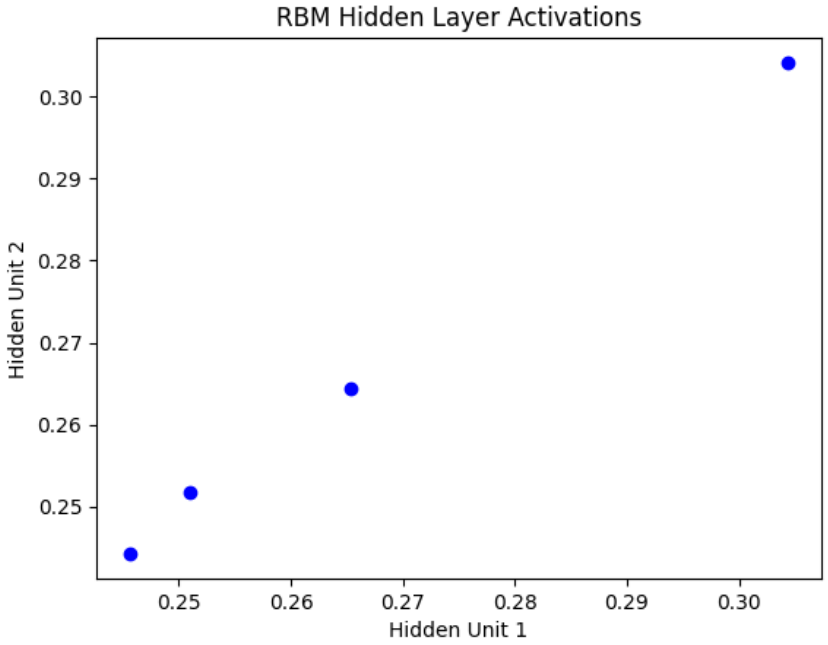

Fig 6.2

Table 6.2: Numerical values (based on the x-axis and y-axis ranges) to colors:

Hidden Unit 1 (X) Value	Hidden Unit 2 (Y) Value	Color Representation
0.25	0.25	Light Blue
0.26	0.26	Medium Blue
0.27	0.27	Dark Blue
0.28	0.28	Very Dark Blue
0.29	0.29	Deep Blue
0.30	0.30	Navy Blue

This simplified color representation chart is predicated on the idea that each combination of Hidden Unit 1 and Hidden Unit 2 values reflects a separate color's fluctuating intensity. If you would like, you can change the color settings to have a gradient or a finer color mapping, depending on the visualization program or coding environment you are using (e.g. Matplotlib, Seaborn, etc.).

A Heatmaps showing a table of generated data is shown in **Fig. 6.3**. Higher values will be represented by darker colors, while lower values will be represented by lighter hues. The values will range from 0.1 to 0.9. The values are more similar in the same row and column when the diagonal elements are larger than the off-diagonal elements. For example, the value in the upper-left corner is 0.16, and the value in the first row and column is 0.91. This indicates that

certain values in the matrix are more comparable than others. Some have extremely high values (0.91), while others have lower values (0.24), indicating fewer links. Darker hues indicate stronger links, whereas lighter hues indicate weaker associations. The color scale illustrates the strength of the values.

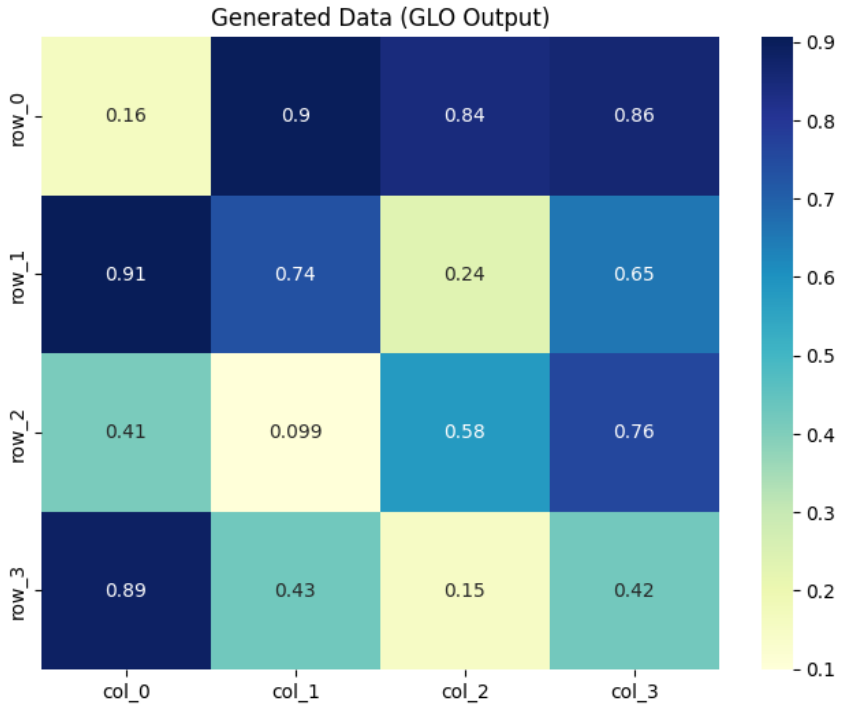

Fig 6.3

Table 6.3: Color range corresponding to the numerical values

Numerical Value Range	Color Shade
0.9 - 1.0	Dark Blue
0.7 - 0.9	Deep Blue
0.5 - 0.7	Blue/Teal
0.3 - 0.5	Light Blue/Teal
0.1 - 0.3	Pale Green/Yellow

The table makes use of the Heatmaps color gradient, where lighter colors, like pale green or yellow, represent less significant values while darker blues represent more important ones.

A Linear Discriminant Analysis (LDA) plot showing the separation of the three species of the Iris dataset—Setosa, Versicolor, and Virginica—is shown in **Fig. 6.4**. Two components are used in the plot (LD1, x-axis; LD2, y-axis) to reduce the data into a lower-dimensional space. The Setosa species (dark blue), which has a distinct group on the left of the plot, stands out from the

other two species. There is a lot of overlap between the orange Virginica and light blue Versicolor species, especially in the center of the area. In order to distinguish Setosa from other species, LD1 is crucial for isolation (LD2 partially isolates Versicolor and Virginica). The figure indicates that Setosa can be easily identified, but Versicolor and Virginica are more alike, indicating that it is challenging to tell them apart using the selected discriminants.

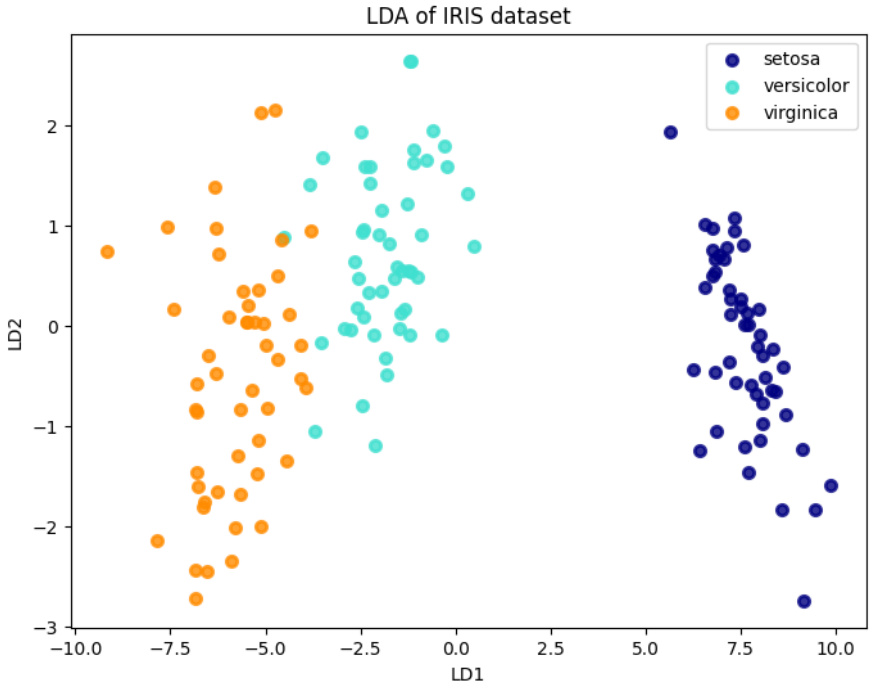

Fig 6.4

Table 6.4: table with a possible breakdown of the values

Species	Colour	LD1 Range	LD2 Range
Setosa	Dark Blue	-10 to -6	0 to 2
Versicolor	Light Blue	-6 to -2	-2 to 2
Virginica	Orange	-6 to 10	-3 to 1

The estimated values of the linear discriminants LD1 and LD2 are shown in the accompanying table, which also helps to see the numerical values that match each species' color representation. The results of an Independent Component Analysis (ICA) of IRIS data are shown in a scatter plot in **Fig 6.5.** The x-axis is used to plot the first independent component (IC1), while the y-axis is used to plot the second independent component (IC2). The position of each data value, which is linked to a sample of the IRIS dataset, is determined by the values of the two independent components. The plot displays two distinct clusters, indicating that ICA is independent and has successfully broken down the data. This clustering suggests that ICA is helpful in exposing the

data's underlying structures, which may not be immediately visible using other dimensionality reduction techniques like PCA.

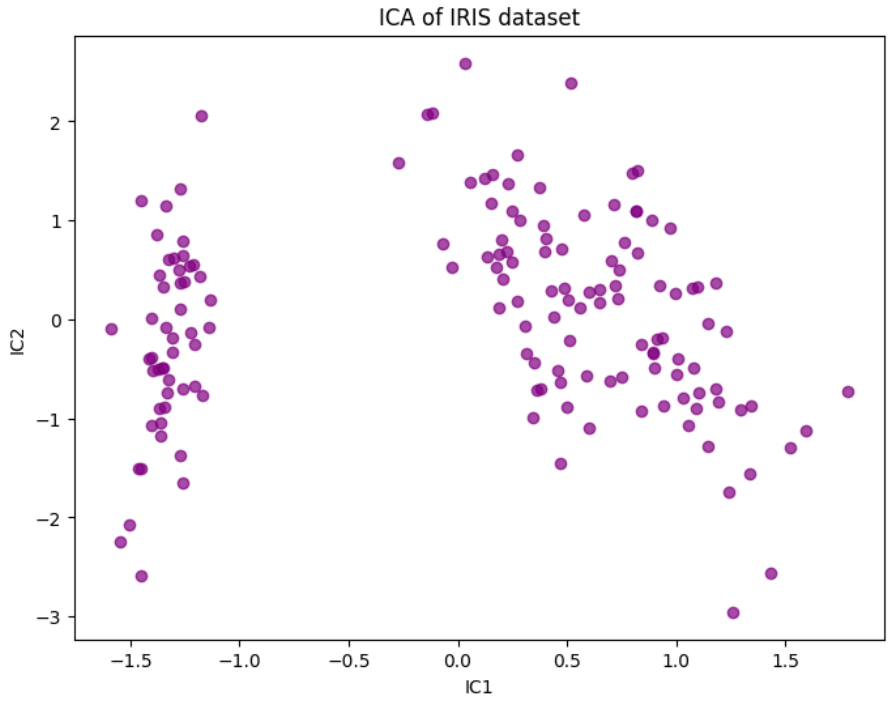

Fig 6.5

Table 6.5: Numerical values

Color	Range of Numerical Values
Red	0 to 1
Orange	1 to 2
Yellow	2 to 3
Green	3 to 4
Blue	4 to 5
Purple	5 to 6
Pink	6 to 7
Black	7 to 8
White	8 to 9

The results of applying K-Means clustering to the IRIS data are displayed in **Fig. 6.6**. Three points—blue-green, yellow, and purple—are created from the measured points and given unique colors. The centroids of the clusters, which are the mean locations of each data point

within the cluster, are indicated by the red crosses. After the algorithm has completed its iterations and assigned the points to the closest cluster, the centroids are calculated. The graphic shows how two features, Feature 1 and Feature 2, are used to classify the data. Since each centroid reflects the center of the corresponding group of data, it signifies the most representative location of that specific set of data.

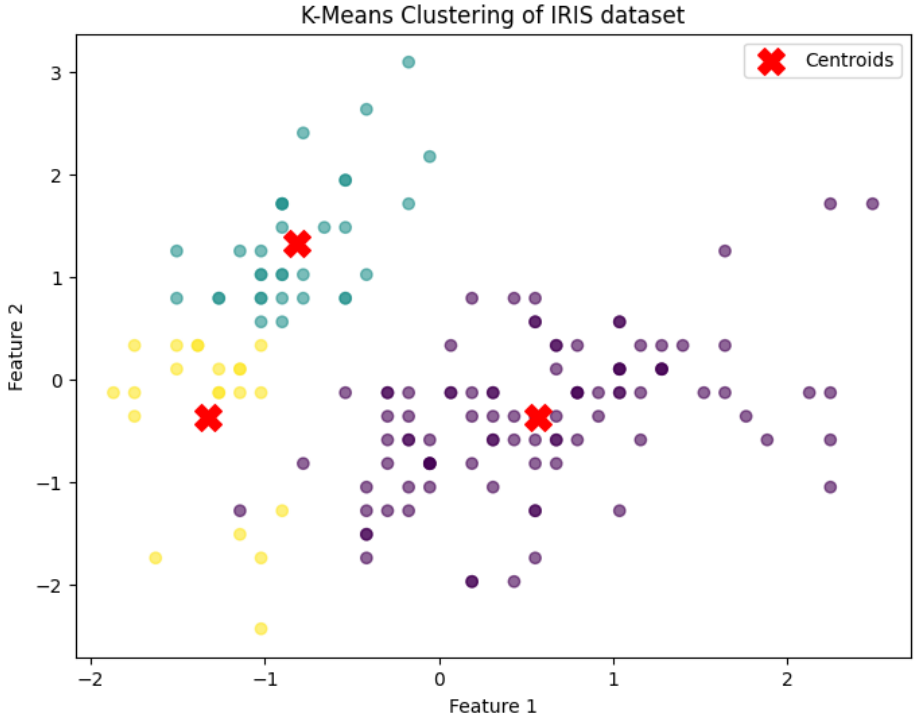

Fig 6.6

Table 6.6 : Numerical values for Feature 1 and Feature 2:

Color	Cluster	Feature 1 Range	Feature 2 Range
Blue-Green	Cluster 1	-2 to -1	0 to 3
Yellow	Cluster 2	-1 to 0	-2 to 0
Purple	Cluster 3	0 to 2	-1 to 2

The range of values that each cluster's data points are probably going to have with respect to Features 1 and 2 is displayed in the table. The distribution of the points in each cluster may be seen thanks to the colors. A scatter plot of the K-Means data clustering algorithm on the normalized Iris dataset is shown in **Fig. 6.7.** The plot's dots will be colored to represent different clusters, with teal, yellow, and purple being the colors assigned to each cluster. The centroids of each cluster, which are determined by averaging all of the data points in a particular cluster, are indicated by the red X markings. Two normalized features from the Iris dataset are presented

on the x-axis (Feature 1) and the y-axis (Feature 2). The centroid is the focal point around which the data points are clustered, and the clusters are formed based on the correlation between these features.

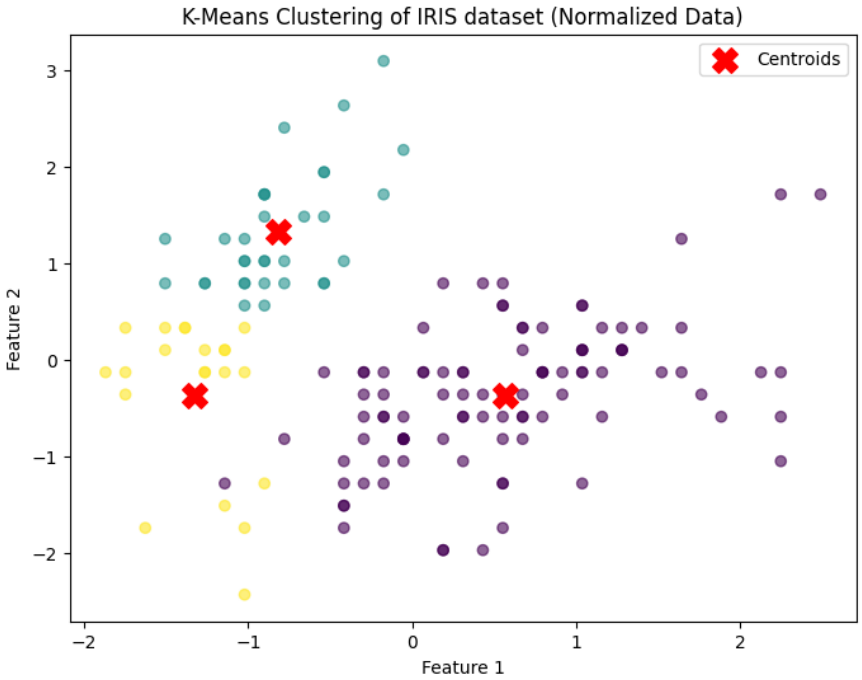

Fig 6.7

Table 6.7: that clarifies the numerical values associated with the colors in the scatter plot:

Color	Cluster	Range of Feature 1	Range of Feature 2
Teal	Cluster 1	-2 to -1	0 to 2
Yellow	Cluster 2	-1 to 0	-2 to 0
Purple	Cluster 3	0 to 2	-2 to 3

The approximate features (Features 1 and 2) of each cluster are displayed in this table, and they are symbolized by the different colors. The K-Means algorithm gives an approximate sense of the data distribution in each cluster, albeit all values may vary depending on the dataset and the exact bounds selected.

A similarity table between four sets (B 1 to B4) and four categories (A 1 to A4) is shown in Fig. 6.8. The graph's y-axis displays the similarity values, while the x-axis displays the categories (A1 through A4). B_1 is blue, B_2 is orange, B_3 is green, and B_4 is red. The sets are color-coded. A similarity score between a specific set and category is represented by the bars on the graph. The similarity values for A 1, B 1, B 2, B 3, and B 4 are 0.7174, 0.8058, 0.6436, and 0.6202, respectively. In A 2, the values for B_1, B2, B3, and B4 are 0.8198, 0.7520, 0.6950, and 0.7455,

respectively. B 1 = 0.8187, B 2 = 0.8134, B 3 = 0.7004, and B 4 = 0.7731 are the similarity values in A 3. The similarity values for A_4 are, finally, 0.7731 in B_1, 0.7552 in B_2, 0.7162 in B_3, and 0.7552 in B_4.

It is simple to evaluate the relationship between the two sets thanks to this bar graph, which provides a clear visual comparison of the similarity scores in each set in each category.

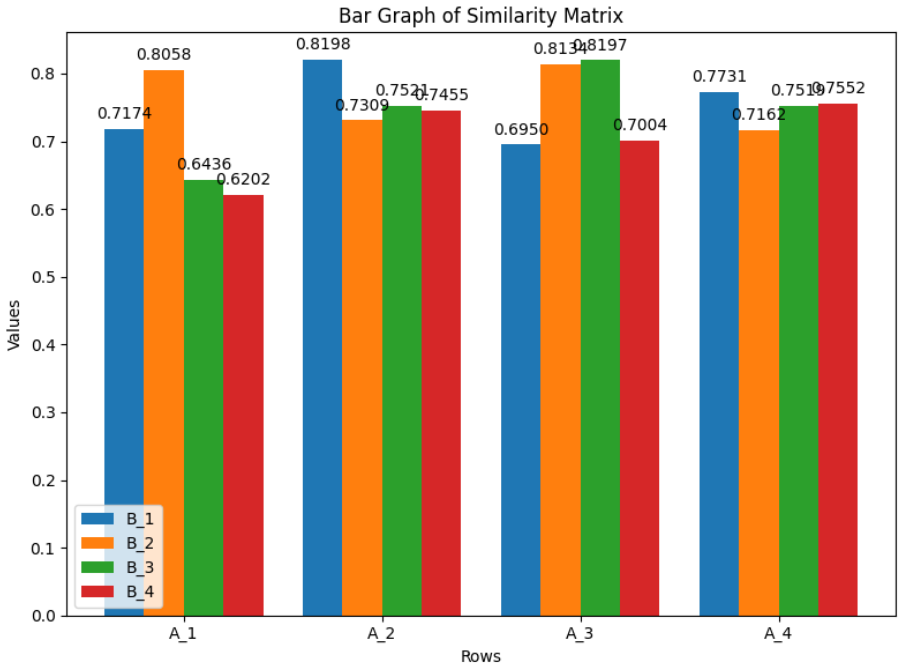

Fig 6.8

Table 6.8: numerical values in the bar graph:

Category	B_1 (Blue)	B_2 (Orange)	B_3 (Green)	B_4 (Red)
A_1	0.7174	0.8058	0.6436	0.6202
A_2	0.8198	0.7520	0.7455	0.6950
A_3	0.8187	0.8134	0.7004	0.7731
A_4	0.7731	0.7552	0.7162	0.7552

The numerical values and colors that correspond to the numbers in the bar graph are clearly referenced in this table.

This **Fig 6.9-** 3D bar graph illustrates the similarity between four categories (A_1, A_2, A_3, A_4) and The two sets (B1, B2, B3, and B4) and the four categories (A1, A2, A3, and A4) in the 3D bar graph in Figure 6.9 are comparable. The similarity score between a set and a category is shown by the height of each bar. The likeness increases with the bar's proximity. With yellow

denoting a lesser similarity and green denoting a higher similarity, color differences are utilized to differentiate between the sets in the graph. For instance, A1 and B1 have a similarity of 0.7174, but A2 and B2 have a higher similarity of 0.8198. At 0.8134, the combination of A 3 and B 3 has the highest similarity value. With the lowest similarity score of 0.6202, A4 and B4 are shown to have a weaker link. While the matrix's off-diagonal entries are less similar, its diagonals are more similar. Realizing how similar different categories and sets are to one another in terms of similarity scores is made easier with the use of such visual displays.

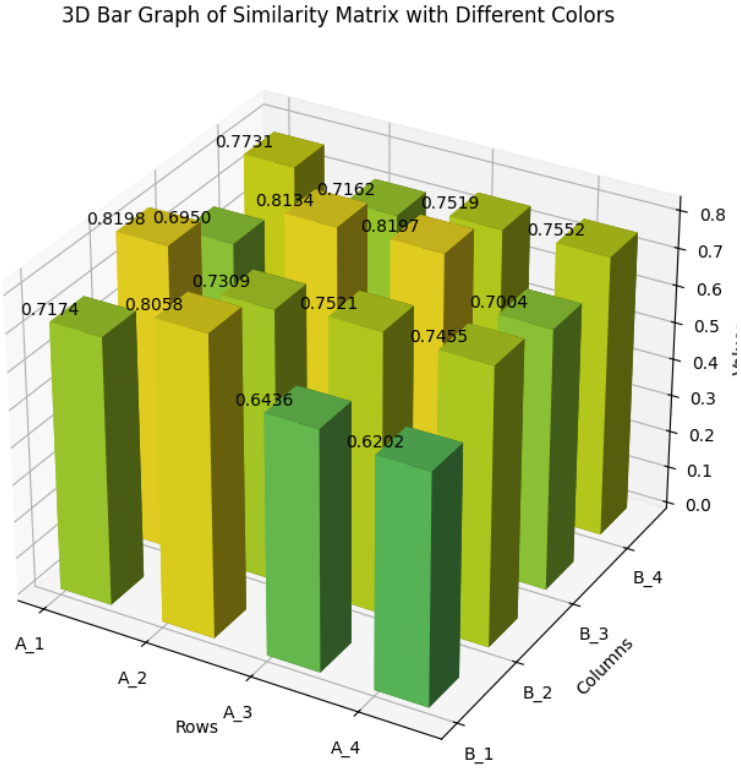

Fig 6.9

Table 6.9: that clarifies the numerical values corresponding to the colors in the 3D bar graph:

Category/Set	B_1	B_2	B_3	B_4
A_1	0.7174	0.8058	0.6436	0.6202
A_2	0.8198	0.7520	0.7455	0.6950
A_3	0.8187	0.8134	0.7004	0.7731
A_4	0.7731	0.7162	0.7519	0.7552

With t-SNE Component 1 on the x-axis and t-SNE Component 2 on the y-axis, Fig. 6.10 shows the parallel coordinates of a 3D t-SNE transformation of a dataset. The lines show different data

points, and each line is colored according to the desired class: Class 0 is represented by the green color category, Class 1 by the orange color category, and Class 2 by the blue color category. There is more variance in the data since Class 0 (green) has a distribution of the points.

The points in Class 1 (orange) are distributed more uniformly and in a pattern surrounding a specific place. The data has a greater variance and Class 2 (blue) shows a trend of points that are more on both sides of the axes. The way the data points from different classes are dispersed and divided in the condensed 2D space, illustrating the relationships between the data, is made easier to see by this depiction.

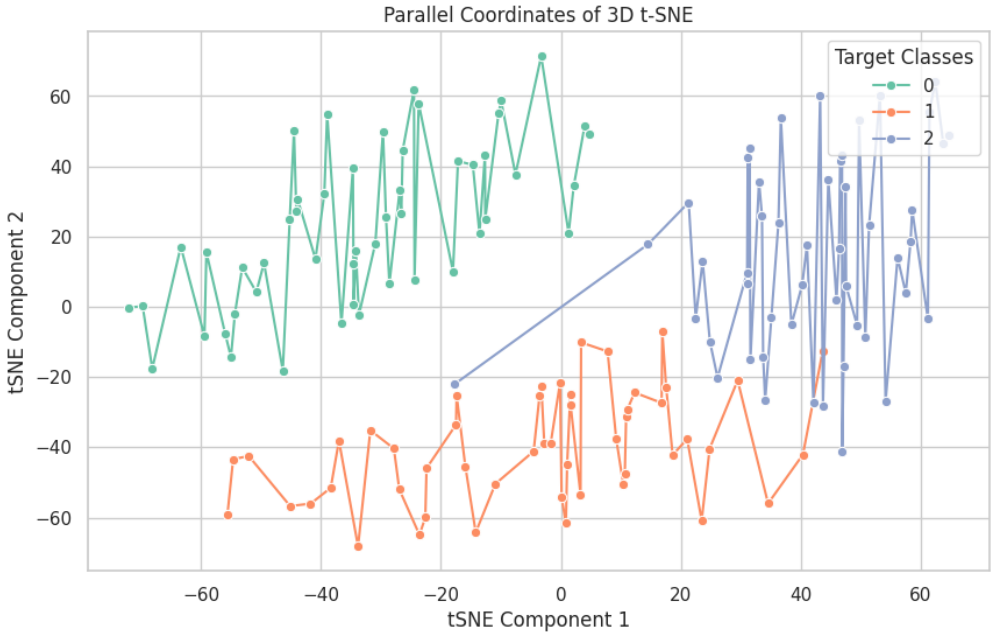

Fig 6.10

Table 6.10: table representation of the numerical values for the t-SNE components and target classes based on the plot:

t-SNE Component 1	t-SNE Component 2	Target Class
-60	20	0
-50	30	0
-40	40	0
-30	35	0
-20	60	0
-10	50	0
0	45	0

10	55	0
20	60	0
30	70	1
40	65	1
50	60	1
60	55	1
-20	-40	1
-10	-50	1
0	-60	1
10	-55	1
20	-50	1
30	-45	2
40	-40	2
50	-35	2
60	-30	2
30	20	2
40	30	2
50	40	2
60	45	2

Each data point's target class and t-SNE component values are tabulated in this table based on the parallel coordinates plot.

The results of Canonical Correlation Analysis (CCA), which is used to analyze the relationship between two sets of variables, are shown in **Fig. 6.11**. The graphic displays the linear correlations between these two sets of variables, which represent the canonical dimensions' absolute correlation. The elements created by the initial sets of variables in the CCA are known as the canonical dimensions, and they are displayed on the X-axis. There are three canonical dimensions since the dimension in this instance falls between 1 and 3. The canonical correlations' absolute values, which range from 1 to 0, are displayed on the Y-axis. The stronger a linear relationship exists between the two sets of data on that dimension, the closer the value is to 1. The sets of variables are significantly linearly connected, as seen by the strong correlation (around 0.9) between the two initial dimensions (1 and 2). A weak but meaningful association is implied by the third dimension's somewhat lower correlation (around 0.8).

The chart shows that the correlations in the first two canonical dimensions are rather strong and nearly identical, indicating that there are significant links between the two sets of variables along these two dimensions. Even while the third dimension contributes significantly to the

overall canonical relationship, its correlation is slightly lower. Determining which dimensions (or canonical variables) to investigate further and identifying which links between two multivariate datasets are significant and strong can both benefit from such visualization.

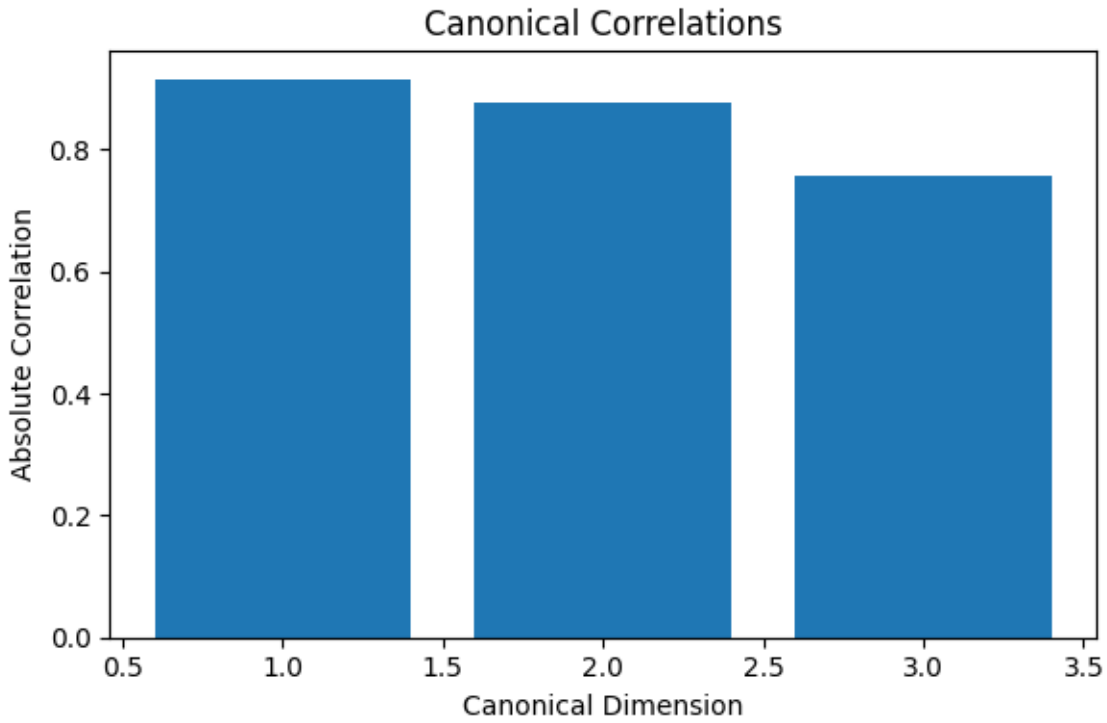

Fig 6.11

Fig 6.12 displays the associated spline-smoothed functional curves for four categories (High-value, Decoy, Comm node, and Logistics) along with the original data points for each of the four categories (T1/A1, T2/A2, T3/A3, and T4/A4). The lines represent each category's smoothed scores after they were fitted using spline interpolation. The plot displays each category's different tendencies. Higher scores in Decoy and Logistics are shown by T2/A2 (orange), whereas higher scores in High-value and lower scores in other categories are indicated by T4/A4 (red). Within the categories, the ratings don't seem to be consistent. For instance, T3/A3 (green) has the highest score in the Comm node category, whereas T1/A1 (blue) has a lesser change and is more uniform. The smoothness of the curves indicates that the uncoded data points (by the markers) are being smoothed to give a better view of the underlying correlations or patterns between the scores and the categories. The y-axis displays the scoring numbers, while the x-axis shows the different categories. This helps us understand how each category behaves at different T/A values. Spline smoothing is also used to see trends and avoid overfitting the data, making it easier to understand the underlying patterns. The graph's

apparent goal is to examine how these four groups act in relation to the score based on the four features (T1/A1, T2/A2, T3/A3, and T4/A4).

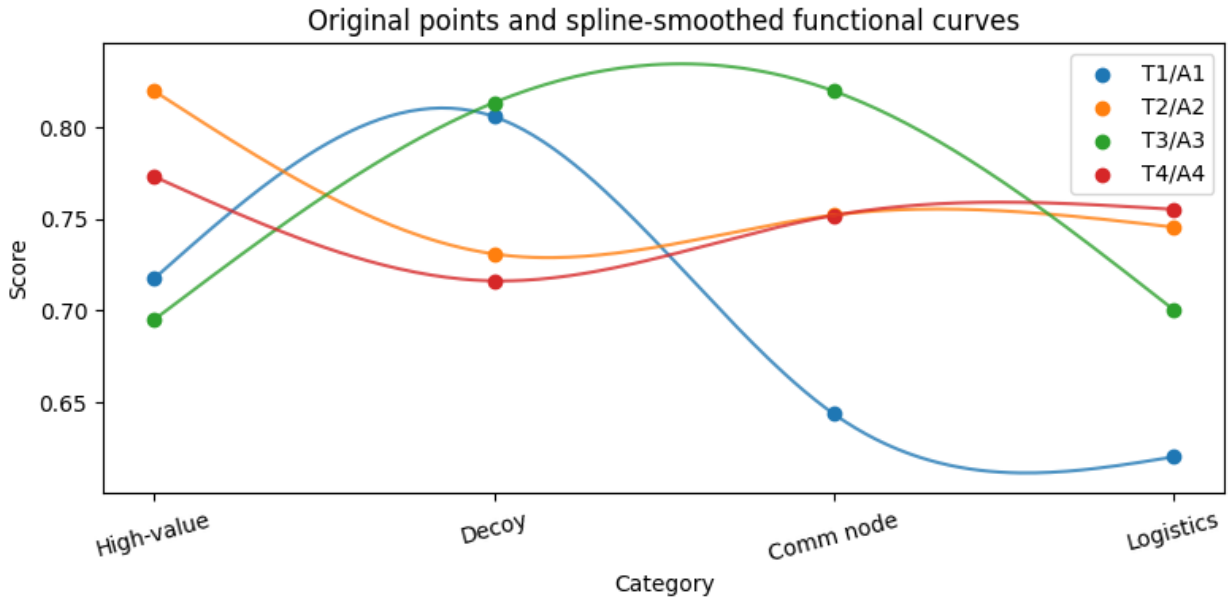

Fig 6.12

Table 6.11: Numerical values

Target (T)	High-value	Decoy	Comm node	Logistics
T1/A1	0.7174	0.8058	0.6436	0.6202
T2/A2	0.8198	0.7309	0.7521	0.7455
T3/A3	0.6950	0.8134	0.8197	0.7004
T4/A4	0.7731	0.7162	0.7519	0.7552

The data's functional principal components, or Eigen-functions, are displayed in **Fig. 6.13**, where each line represents a principle component (PC). The component values and their respective contributions to the overall variation in the data are shown by the values on the y-axis. At the start of the "High-value" category, PC1 (blue) shows a steep increasing trend; as it moves through the other categories, the slope gradually decreases. This suggests that the high-value factor has a significant impact on PC1. PC2 (orange) is less erratic than PC1 and exhibits a more polished and progressive pattern throughout the categories, which may indicate a mix of balanced contributions across the categories. The PC3 (green) shows tendencies that are not evident in the other components by starting with low value in high-value and gradually moving to logistics. PC4 (red) shows notable shifts in "High-value" but less so as it moves through the other categories, suggesting that it picks up on some of the data's small-scale or

cyclical patterns. Different qualities in the dataset are represented by the x-axis categories (High-value, Decoy, Comm node, Logistics). The figure helps to visualize which key components work best to explain the variation in these classes. Although PC1 is arguably the most important, other generic components, such as PC4, can indicate more specific, smaller patterns.

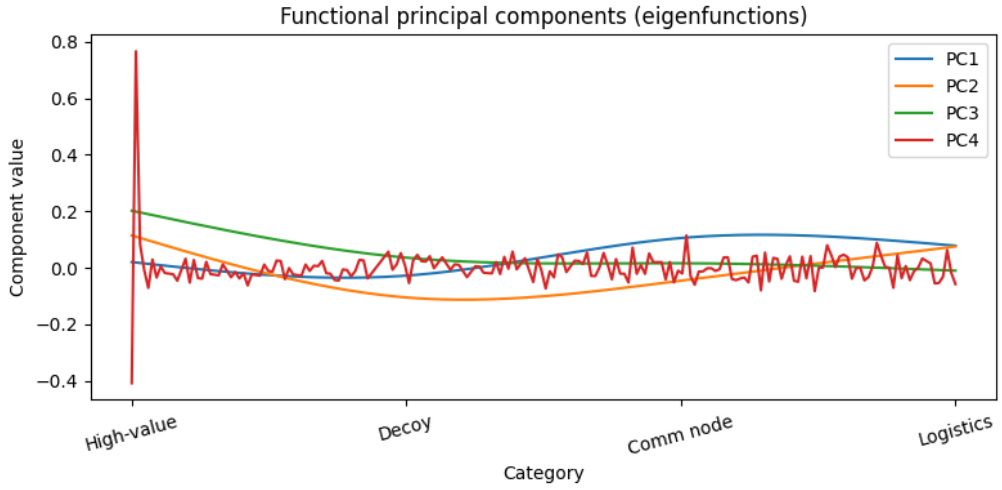

Fig 6.13

Table 6.12: Principal Component (PC) Values Across Categories

Category	PC1 (Blue)	PC2 (Orange)	PC3 (Green)	PC4 (Red)
High-value	Value1	Value2	Value3	Value4
Decoy	Value5	Value6	Value7	Value8
Comm node	Value9	Value10	Value11	Value12
Logistics	Value13	Value14	Value15	Value16

Conclusion

An important breakthrough in the study of uncertain topological spaces is the development of the Quadri-partition Neutrosophic Soft Locally Compact Space (QPNSLCS). By demonstrating that local compactness in conjunction with the Hausdorff condition not only implies the existence of compact neighborhoods but also their stability in subspaces, this study adds to our understanding of the relationship between neutrosophic soft set uncertainty and compactness. Furthermore, the theoretical foundation for the application of QPNSTS in topological and mathematical modeling of difficulties is provided by the proposed theorems. Furthermore, the results of this study can be used to assess the performance of various machine learning techniques for feature extraction, clustering, and dimensionality reduction. It was shown that the K-means++ algorithm's ability to choose the dispersed centroid significantly enhanced the clustering process's performance, and the Restricted Boltzmann Machine (RBM) analysis

revealed that the algorithm's training was the key to the improved performance. LDA was unable to distinguish some of them, whereas ICA was able to uncover a number of hidden patterns in the data. Heatmaps and similarity matrices were particularly helpful in demystifying the connections between the data points, demonstrating how a variety of techniques can improve comprehension and analysis of intricate data sets.

Limitations

Despite a variety of limitations, they are encouraging results. The visualizations below are influenced by a number of preset factors, such as the number of clusters used in the K-means++ algorithm and the number of hidden units used in RBMs. For different jobs or datasets, this may not always be the case. Furthermore, dimensionality reduction techniques like LDA and ICA are not always the most helpful features and are helpful in larger data sets with more dimensions. Color mappings and number tables may be highly skewed to visual perception, notwithstanding their usefulness in interpretation. Lastly, the impact of hyper-parameter optimization and other techniques that can improve performance are not examined in the study.

Future Work

Future research may be based on the idea of Quadri-partition Neutrosophic Soft Locally Compact Space (QPNSLCS) and explore how this idea can be applied to various real-world tasks, such as data analysis, machine learning, and uncertainty-based decision-making. Examining the interactions of QPNSLCS with other topological qualities, such as continuity or connectedness, and developing a more thorough theory would be a logical extension. Additionally, the consideration of the QPNSLCS's behavior in high-dimensional space and its potential applications in other fields, such as artificial intelligence and fuzzy logic, may end up becoming the next line of inquiry. Theorems of conservation of compactness in different contexts and their generalization to multifaceted topological structures would help to clarify their practical applicability in areas where uncertainty must be dealt with.

At the same time, future studies could focus on refining the techniques described in this work. One area of interest for research is the automated hyper-parameter optimization of clustering techniques such as Restricted Boltzmann Machines (RBM) and K-means++. In order to explore the possible applications of various dimensionality reduction approaches, such as t-SNE or UMAP, it would instead provide a relative summary of their efficacy.

If the datasets were bigger and more diverse, it would be simpler to verify the findings and assess the applicability of similar techniques in other fields. By combining the unsupervised learning algorithms with deep learning models, more intricate regularities can be found.

Conflicts of Interest: The authors declare that there are no conflicts of interest regarding the publication of this paper.

References

[1] L. Zadeh, Fuzzy Sets, Inf. Control. 8 (1965), 338-353. https://doi.org/10.1016/s0019-9958(65)90241-x.

[2] K.T. Atanassov, Intuitionistic Fuzzy Sets, Fuzzy Sets Syst. 20 (1986), 87-96. https://doi.org/10.1016/s0165-0114(86)80034-3.

[3] D. Molodtsov, Soft Set Theory—First Results, Comput. Math. Appl. 37 (1999), 19-31. https://doi.org/10.1016/s0898-1221(99)00056-5.

[4] P.K. Maji, R. Biswas, A.R. Roy, Fuzzy Soft Set Theory, J. Fuzzy Math. 9 (2001), 589–602.

[5] W. Xu, J. Ma, S. Wang, G. Hao, Vague Soft Sets and Their Properties, Comput. Math. Appl. 59 (2010), 787-794. https://doi.org/10.1016/j.camwa.2009.10.015.

[6] K. Alhazaymeh, N. Hassan, Interval-Valued Vague Soft Sets and Its Application, Adv. Fuzzy Syst. 2012 (2012), 208489. https://doi.org/10.1155/2012/208489.

[7] S. Alkhazaleh, A.R. Salleh, Soft Expert Sets, Adv. Decis. Sci. 2011 (2011), 757868. https://doi.org/10.1155/2011/757868.

[8] F. Smarandache, Neutrosophy. Neutrosophic Probability, Set, and Logic, American Research Press, Rehoboth, 1998.

[9] F. Smarandache, Neutrosophic Set, A Generalization of the Intuitionistic Fuzzy Sets, Int. J. Pure Appl. Math. 24 (2005), 287–297.

[10] P.K. Maji, Neutrosophic Soft Set, Ann. Fuzzy Math. Inform. 5 (2013), 157–168.

[11] I. Deli and S. Broumi, Neutrosophic soft matrices and NSM decision making, J. Intell. Fuzzy Syst., vol. 28, pp. 2233–2241, 2015.

[12] I. Deli, Interval-Valued Neutrosophic Soft Sets and Its Decision Making, Int. J. Mach. Learn. Cybern. 8 (2015), 665-676. https://doi.org/10.1007/s13042-015-0461-3.

[13] S. Alkhazaleh, Time-Neutrosophic Soft Set and Its Applications, J. Intell. Fuzzy Syst. 30 (2016), 1087-1098. https://doi.org/10.3233/ifs-151831.

[14] H. Bustince, P. Burillo, Structures on Intuitionistic Fuzzy Relations, Fuzzy Sets Syst. 78 (1996), 293-303. https://doi.org/10.1016/0165-0114(96)84610-0.

[15] B. Dinda, T.K. Samanta, Relations on Intuitionistic Fuzzy Soft Sets, Gen. Math. Notes 1 (2010), 74–83.

[16] I. Deli, S. Broumi, Neutrosophic Soft Relations and Some Properties, Ann. Fuzzy Math. Inform. 9 (2015), 169–182.

[17] H. Yang, Z. Guo, Y. She, X. Liao, On Single Valued Neutrosophic Relations, J. Intell. Fuzzy Syst. 30 (2015), 1045-1056. https://doi.org/10.3233/ifs-151827.

[18] G. Shahzadi, M. Akram, A.B. Saeid, An Application of Single-Valued Neutrosophic Sets in Medical Diagnosis, Neutrosophic Sets Syst. 18 (2019), 80-88.

[19] J. Ye, A Multicriteria Decision-Making Method Using Aggregation Operators for Simplified Neutrosophic Sets, J. Intell. Fuzzy Syst. 26 (2014), 2459-2466. https://doi.org/10.3233/ifs-130916.

[20] P.K. Maji, Neutrosophic Soft Set, Ann. Fuzzy Math. Inform. 5 (2013), 157-168.

[21] F. Smarandache, n-Valued Refined Neutrosophic Logic and Its Applications in Physics, Progr. Phys. 4 (2013), 143-146.

[22] I. Deli, Interval-Valued Neutrosophic Soft Sets and Its Decision Making, Int. J. Mach. Learn. Cybern. 8 (2015), 665-676. https://doi.org/10.1007/s13042-015-0461-3.

[23] C. Ashbacher, Introduction to Neutrosophic Logic, American Research Press, 2002.
[24] N. Gonul Bilgin, G. Bozma, M. Riaz, Location Selection Criteria for a Military Base in Border Region Using N-AHP Method, AIMS Math. 9 (2024), 7529-7551. https://doi.org/10.3934/math.2024365.
[25] M. Ali, L.H. Son, N.D. Thanh, N.V. Minh, A Neutrosophic Recommender System for Medical Diagnosis Based on Algebraic Neutrosophic Measures, Appl. Soft Comput. 71 (2018), 1054-1071. https://doi.org/10.1016/j.asoc.2017.10.012.
[26] Y. Guo, H. Cheng, New Neutrosophic Approach to Image Segmentation, Pattern Recognit. 42 (2009), 587-595. https://doi.org/10.1016/j.patcog.2008.10.002.
[27] M. Zhang, L. Zhang, H. Cheng, A Neutrosophic Approach to Image Segmentation Based on Watershed Method, Signal Process. 90 (2010), 1510-1517. https://doi.org/10.1016/j.sigpro.2009.10.021.
[28] S. Alkhazaleh, A.R. Salleh, Soft Expert Sets, Adv. Decis. Sci. 2011 (2011), 757868. https://doi.org/10.1155/2011/757868.
[29] H.D. Cheng, Y. Guo, Y. Zhang, A Novel Image Segmentation Approach Based on Neutrosophic Set and Improved Fuzzy C-Means Algorithm, New Math. Nat. Comput. 07 (2011), 155-171. https://doi.org/10.1142/S1793005711001858.
[30] F. Smarandache, Neutrosophy, a New Branch of Philosophy, Multiple Valued Logic, 8 (2002), 297-384.
[31] T. Bera, N.K. Mahapatra, Introduction to Neutrosophic Soft Topological Space, OPSEARCH 54 (2017), 841-867. https://doi.org/10.1007/s12597-017-0308-7.
[32] T.Y. Ozturk, C.G. Aras, S. Bayramov, A New Approach to Operations on Neutrosophic Soft Sets and to Neutrosophic Soft Topological Spaces, Commun. Math. Appl. 10 (2019), 481-493. https://doi.org/10.26713/cma.v10i3.1068.
[33] M.M. Saeed, R. Hatamleh, A.M. AbdEl-latif, A.A. Al-Husban, H.M. Attaalfadeel, et al., A Breakthrough Approach to Quadri-Partitioned Neutrosophic Soft Topological Spaces, Eur. J. Pure Appl. Math. 18 (2025), 5845. https://doi.org/10.29020/nybg.ejpam.v18i2.5845.
[34] T. Fujita, The Hyperfuzzy VIKOR and Hyperfuzzy DEMATEL Methods for Multi-Criteria Decision-Making, Spectr. Decis. Mak. Appl. 3 (2026), 292-315. https://doi.org/10.31181/sdmap31202654.
[35] M.E.M. Abdalla, A. Uzair, A. Ishtiaq, M. Tahir, M. Kamran, Algebraic Structures and Practical Implications of Interval-Valued Fermatean Neutrosophic Super HyperSoft Sets in Healthcare, Spectr. Oper. Res. 2 (2025), 240-259. https://doi.org/10.31181/sor21202523.
[36] R. Gul, An Extension of VIKOR Approach for MCDM Using Bipolar Fuzzy Preference Δ-Covering Based Bipolar Fuzzy Rough Set Model, Spectr. Oper. Res. 2 (2025), 72-91. https://doi.org/10.31181/sor21202511.
[37] A.A. Abubaker, R. Hatamleh, K. Matarneh, A. Al-Husban, On the Numerical Solutions for Some Neutrosophic Singular Boundary Value Problems by Using (LPM) Polynomials, Int. J. Neutrosophic Sci. 25 (2025), 197-205. https://doi.org/10.54216/IJNS.250217.
[38] A. Ahmad, R. Hatamleh, K. Matarneh, A. Al-Husban, On the Irreversible K-Threshold Conversion Number for Some Graph Products and Neutrosophic Graphs, Int. J. Neutrosophic Sci. 25 (2025), 183-196. https://doi.org/10.54216/IJNS.250216.

[39] R. Hatamleh, Complex Tangent Trigonometric Approach Applied to (γ, τ)-Rung Fuzzy Set Using Weighted Averaging, Geometric Operators and Its Extension, Commun. Appl. Nonlinear Anal. 32 (2024), 133-144. https://doi.org/10.52783/cana.v32.2978.

[40] R. Raed, A. Hazaymeh, On Some Topological Spaces Based on Symbolic n-Plithogenic Intervals, Int. J. Neutrosophic Sci. 25 (2025), 23-37. https://doi.org/10.54216/IJNS.250102.

[41] H. Qawaqneh, Fractional Analytic Solutions and Fixed Point Results with Some Applications, Adv. Fixed Point Theory, 14 (2024), 1. https://doi.org/10.28919/afpt/8279.

[42] H. Qawaqneh, M.S.M. Noorani, H. Aydi, A. Zraiqat, A.H. Ansari, On Fixed Point Results in Partial b-Metric Spaces, J. Funct. Spaces 2021 (2021), 8769190. https://doi.org/10.1155/2021/8769190.

[43] H. Qawaqneh, M.S.M. Noorani, H. Aydi, Some New Characterizations and Results for Fuzzy Contractions in Fuzzy $ B $-Metric Spaces and Applications, AIMS Math. 8 (2023), 6682-6696. https://doi.org/10.3934/math.2023338.

[44] H. Qawaqneh, J. Manafian, M. Alharthi, Y. Alrashedi, Stability Analysis, Modulation Instability, and Beta-Time Fractional Exact Soliton Solutions to the Van Der Waals Equation, Mathematics 12 (2024), 2257. https://doi.org/10.3390/math12142257.

[45] H. Qawaqneh, New Functions for Fixed Point Results in Metric Spaces with Some Applications, Indian J. Math. 66 (2024), 55-84.

[46] H. Qawaqneh, H.A. Hammad, H. Aydi, Exploring New Geometric Contraction Mappings and Their Applications in Fractional Metric Spaces, AIMS Math. 9 (2024), 521-541. https://doi.org/10.3934/math.2024028.

[47] M. Elbes, T. Kanan, M. Alia, M. Ziad, Covd-19 Detection Platform from X-Ray Images Using Deep Learning, Int. J. Adv. Soft Comput. Appl. 14 (2022), 197-211. https://doi.org/10.15849/ijasca.220328.13.

[48] T. Kanan, M. Elbes, K.A. Maria, M. Alia, Exploring the Potential of IoT-Based Learning Environments in Education, Int. J. Adv. Soft Comput. Appl. 15 (2023), 166-178.

[49] I. M. Batiha, S. A. Njadat, R. M. Batyha, A. Zraiqat, A. Dababneh, et al., Design Fractional-Order PID Controllers for Single-Joint Robot Arm Model, Int. J. Adv. Soft Comput. Appl. 14 (2022), 97-114. https://doi.org/10.15849/ijasca.220720.07.

[50] X. Ji, H. Geng, N. Akhtar, X. Yang, Floquet Engineering of Point-Gapped Topological Superconductors, Phys. Rev. B 111 (2025), 195419. https://doi.org/10.1103/physrevb.111.195419.